



INCLUSION OF MEASURED FREQUENCY- AND AMPLITUDE-DEPENDENT MOUNT PROPERTIES IN VEHICLE OR MACHINERY MODELS

T. JEONG AND R. SINGH

Acoustics and Dynamics Laboratory, Department of Mechanical Engineering and The Center for Automotive Research, The Ohio State University, Columbus, OH 43210-1107, U.S.A.

(Received 2 December 1999, and in final form 5 June 2000)

This article proposes several new or refined analytical methods for vehicle or machinery system models that include measured dynamic stiffness of vibration isolators or mounts. Complications arising due to the spectrally varying and/or amplitude-dependent parameters are categorized, and the associated eigenvalue and frequency response problems are defined. First, the real and complex eigenvalue problems that include both viscous and visco-elastic damping models are critically examined and illustrated via examples. Second, a non-linear eigenvalue problem is formulated and the resulting eigensolutions are determined for a two-degree-of-freedom system with frequency-dependent elastic and dissipative parameters. Several approximate methods, including the modal expansion method, are also proposed to calculate the forced harmonic response, and their solution errors are assessed. Third, a quasi-linear method is applied to a 1/2 car model, using measured data of a typical hydraulic engine mount, to see the effect of excitation amplitude-dependent dynamic stiffnesses. Finally, a refined non-linear, frequency domain synthesis method is proposed that includes local non-linearities in the form of measured dynamic stiffness data. The forced harmonic response of the overall system is obtained, and comparing to the corresponding time domain method for a specific 1/4 car vehicle model validates it.

© 2001 Academic Press

1. INTRODUCTION

Stiffness and damping rates of practical elastomeric isolators, hydraulic mounts and the like depend on frequency and amplitude of the dynamic excitation, temperature, visco-elastic material or fluid properties, geometrical shape factors, static preload, and even the duration of time under which mounts have been operated [1–3]. Since these properties are difficult to analytically predict, experimental methods must be often adopted for the dynamic characterization or system identification [4–6]. One most common method is the electrohydraulic dynamic (non-resonant) test system that determines the dynamic stiffness $\tilde{K}_d(\omega, X) = \tilde{F}_T/\tilde{X}$ at given excitation frequency ω (rad/s) and displacement amplitude X , while being subjected to a specific static load \bar{f} or displacement as shown in Figure 1 [7, 8]. Here, \sim denotes a complex-valued quantity and the $e^{i\omega t}$ form is used for harmonic signals since sub- and super-harmonics are usually ignored in experimental tests. The measured spectra like those shown in Figure 2 form the basis of design work in most applications including the automotive systems. One may also employ the Voigt model approximation to find equivalent stiffness k and viscous damping coefficient c as a function of ω for any given X [9, 10]. However, such spectrally varying properties pose difficulties since the common analytical tools and computational methods are based on the linear

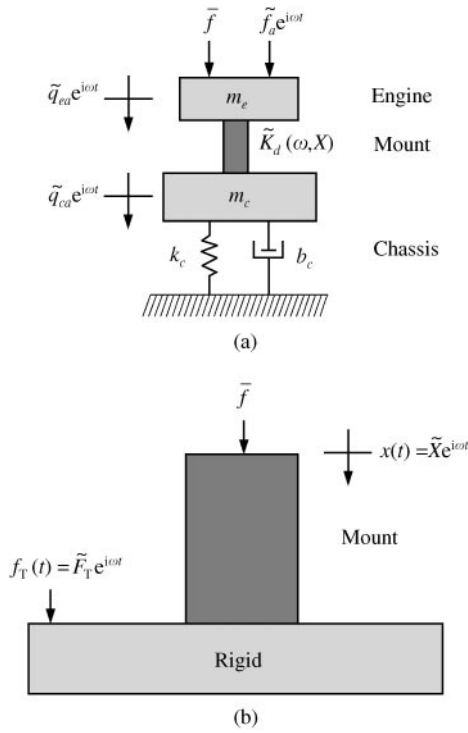


Figure 1. Engine mounting system. (a) Simplified 1/4 car model illustrating engine-mount-chassis system, (b) mount test concept.

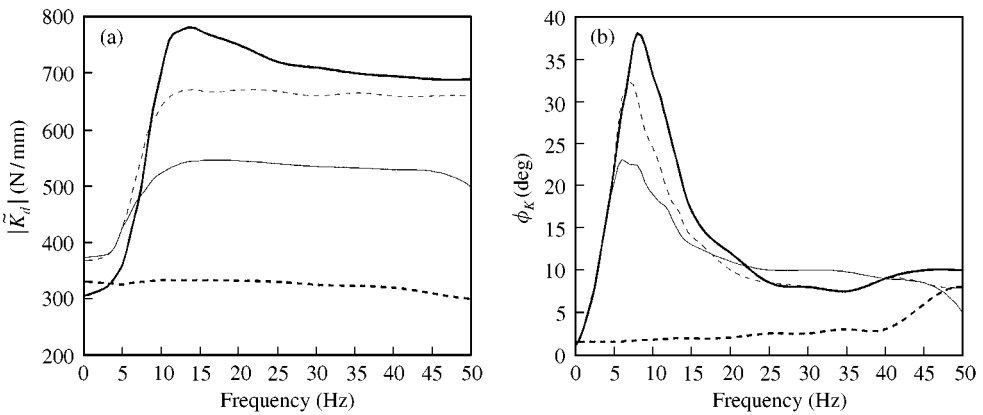


Figure 2. The effect of excitation amplitude X on the measured dynamic stiffness of a hydraulic engine mount (A): - - -, $X = 0.1$ mm; —, $X = 1$ mm; - - -, $X = 2$ mm; —, $X = 3$ mm [8].

time-invariant (LTI) system theory, and the formulations require spectrally invariant values of parameters.

This article intends to develop several analytical methods that may permit the inclusion of $\tilde{K}_d(\omega, X)$ data in lumped parameter-type dynamic simulation models. Several types of the visco-elastic eigenvalue and frequency response problems will be proposed, and examples include both machinery and vehicle models that incorporate $\tilde{K}_d(\omega, X)$ data.

2. PROBLEM FORMULATION

2.1. CLASSIFICATION OF PROBLEMS

The concept of complex dynamic stiffness has been used for over five decades to describe the dynamic behavior of materials and vibration control devices [10–12] since Kimball and Lovell suggested the concept of solid damping in 1927 [13]. Elastomeric isolators, free layer or constrained layer damping treatments, hydraulic mounts and the like often exhibit frequency- and amplitude-dependent behavior. The dry friction and hysteretic damping type phenomena have also been characterized in a similar manner [9, 14–16]. Table 1 summarizes five fundamental problems that are of interest, and each has been discussed in the existing literature to some extent. The following expression may be used to define the stiffness modulus $|\tilde{K}_d| = K'_d\sqrt{1 + \eta^2}$ and loss angle $\phi_K = \tan^{-1} \eta$, where K' is the storage stiffness, K'' is the loss stiffness and η is the loss factor:

$$\tilde{K}_d(\omega, X) = K'_d(\omega, X) + iK''_d(\omega, X) = K'_d(\omega, X)[1 + i\eta(\omega, X)] = |\tilde{K}_d(\omega, X)|e^{i\phi_K(\omega, X)}. \quad (1)$$

Note that two definitions have been used in the literature to define the dynamic stiffness term. The first definition deals with the \tilde{K}_d concept that is shown in Figure 1(a) and via equation (1). The second definition is employed in conventional analytical, computational or experimental vibration or modal analysis where the dynamic stiffness or system matrix for the LTI system is defined as $\mathbf{D} = \mathbf{K}_s - \omega^2\mathbf{M} + i\omega\mathbf{C}$, where \mathbf{K}_s , \mathbf{M} and \mathbf{C} are static stiffness, mass and viscous damping matrices [17]. Both will be used in our analysis.

Specific visco-elastic models may be also employed in developing the classifications of Table 1. Relevant problems will be discussed further in subsequent sections, along with an appropriate review of literature. (Given the comprehensive scope of inquiry, only representative articles will be cited.)

Physical mechanisms that generate frequency- and amplitude-dependent properties in real-life devices and materials differ but their manifestations in the frequency domain may be similar in nature. Also, users may substitute one device or material over the other, often relying on the measured properties. Yet another issue is the variation of system parameters with respect to ω or X . For example, expand $K'_d(\omega, X)$ or $\eta(\omega, X)$ using the

TABLE 1

Classification of relevant problems

Given	Dynamic system type	Typical examples
$K'_d \neq K'_d(\omega, X)$ $\eta \neq \eta(\omega, X)$	Linear time-invariant system	Metallic mounts and structures [5]
$K'_d = K'_d(\omega)$ $\eta = \eta(\omega)$	Linear system with spectrally varying properties	Visco-elastic damping layers [12] Laminated composite panels [15]
$K'_d = K'_d(\omega; X_o)$ $\eta = \eta(\omega; X_o)$	Quasi-linear system	Assumed model for non-linear mounts [8]
$K'_d = K'_d(X)$ $\eta = \eta(X)$	Non-linear system with spectrally invariant properties	Systems with clearances [18] Continuous non-linearities (hardening or softening springs) [19]
$K'_d = K'_d(\omega, X)$ $\eta = \eta(\omega, X)$	Non-linear system with spectrally varying properties	Hydraulic mounts [8] Powertrain clutches [20]

K'_d = storage stiffness; η = loss factor; ω = frequency (rad/s); X = excitation amplitude.

Taylor series

$$K'_d(\omega, X) = K'_d(\omega_o, X_o) + (\omega - \omega_o) \left. \frac{\partial K'_d}{\partial \omega} \right|_{\omega=\omega_o}^{X=X_o} + (X - X_o) \left. \frac{\partial K'_d}{\partial X} \right|_{\omega=\omega_o}^{X=X_o} + O(\Delta\omega^2, \Delta X^2). \quad (2)$$

This illustrates that if changes are rather small, then one may develop suitable analytical approximations. Figure 2, however, shows that changes with ω and X are rather large since $\tilde{K}_d(\omega, X)$ varies from 300 to 780 N/mm in modulus and from 2 to 38° in loss angle. Mostly frequency variations will be discussed in this article though amplitude-dependent cases are also addressed.

2.2. SCOPE AND OBJECTIVES

The scope of this article is limited to the frequency domain analysis, and only lumped parameter models will be employed to illustrate the issues and methodology. Specific objectives are as follows. (1) Clarify and formulate various types of eigenvalue problems including the non-linear case given $\tilde{\mathbf{K}}_d = \tilde{\mathbf{K}}_d(\omega)$, and examine the resulting real or complex eigensolutions. (2) Examine the validity of the modal expansion method for frequency response calculations for various cases of $\tilde{\mathbf{K}}_d(\omega)$. (3) Determine the applicability of using quasi-linear system models that may incorporate measured data $\tilde{K}_d(\omega; X_o)$. (4) Propose a refined synthesis method to obtain the forced harmonic response when $\tilde{K}_d(\omega, X)$ type properties are included in a system model.

The generic machinery isolation system of Figure 3 will be examined first to illustrate the analytical procedures and applications to machinery problems. Figure 1(a) and 4 illustrate vehicle models that will be employed as examples. In Figure 1(a), only the vertical motions are calculated, and the engine is described by a rigid mass m_e . The chassis may be modelled by a linear Voigt model (as shown) or by alternate formulation in terms of equivalent mass \mathbf{M}_c , viscous damping \mathbf{C}_c and stiffness \mathbf{K}_{sc} matrices. Figure 4 shows the 1/2 car model where different degrees of freedom (d.o.f.) may be assigned. In our example, this will be a six-d.o.f. system since only the vertical displacements are chosen.

One key issue that will be discussed later can be illustrated via the vehicle model of Figure 1(b) where $x(t)$ corresponds to $q_e(t) - q_c(t)$ of Figure 1(a). Both q_e and q_c need to be solved for in a simulation program but if the measured mount data were to be included in terms of $\tilde{K}_d(\omega, X)$, numerical iterations are necessary. It should be also pointed out that true non-linear analyses are very difficult since the experimental procedures provide only the “black-box” information, primarily in the frequency domain, while ignoring sub- and super-harmonics [10].

3. LTI VISCO-ELASTIC MODELS

3.1. LITERATURE REVIEW

The single-d.o.f. viscous damping models have often been used to analyze the solid damping phenomena, based on the energy-equivalent viscous damping coefficient concept, even though the dynamic response of the system may be quite different [15]. To overcome this discrepancy, dynamic stiffness \tilde{K}_d formulation [9, 11, 21] may be used to model the solid, structural, hysteretic, or visco-elastic dampings. However, the employment of \tilde{K}_d prevents one from analyzing the transient response of the system since the resulting time

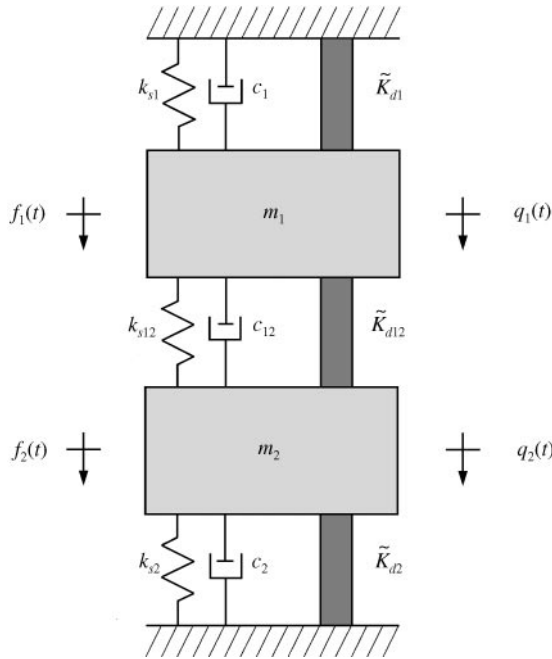


Figure 3. Two degree-of-freedom machinery isolation system with visco-elastic elements as described by dynamic stiffnesses (\tilde{K}_d). These are in parallel with static stiffness (k_s) and viscous damping (c) elements.

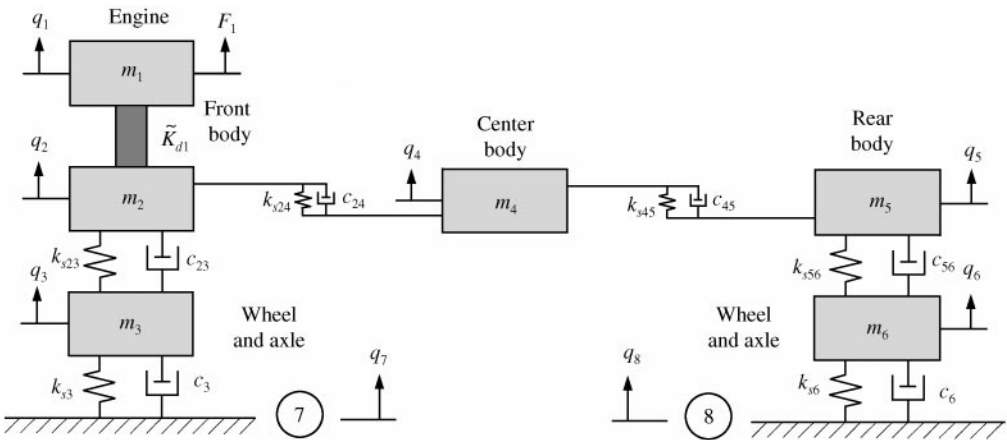


Figure 4. Simplified 1/2 car model. Degrees of freedom may be assigned depending on the frequency range of interest and analysis objective. Other versions such as 1/4 car model are subsets of this case. \tilde{K}_{d1} = measured dynamic stiffness (modulus and loss angle) at any given frequency.

domain model is non-casual [22]. Hence, the \tilde{K}_d concepts should only be used in the ω domain, and only the steady state responses must be sought. Such damping models may be extended to a multi-d.o.f. system and the associated eigenvalue problem can be formulated. The classical modal analysis method, based on the viscous damping assumption, is also applicable to structurally or visco-elastically damped system under certain conditions [16].

Voigt, Maxwell, or Burgers models are subsets of a more general linear visco-elastic model, which is usually defined by the n th order differential equation in terms of both dynamic displacement (or strain) and force (or stress) [9, 12]. Among them, the Voigt model is most widely used because of its simplicity [9, 10]. Hence, this article will only employ the Voigt-type model for multi-d.o.f. dynamic systems, when the need arises.

3.2. FORMULATION

3.2.1. LTI viscous damping models

Only harmonic excitation ($\mathbf{f}(t) = \tilde{\mathbf{f}}_a e^{i\omega t}$) and response ($\mathbf{q}(t) = \tilde{\mathbf{q}}_a e^{i\omega t}$) at ω are considered in this study. The mass matrix (\mathbf{M}) is assumed to be spectrally invariant. The equations of motions for a discrete system of dimension N are

$$\mathbf{M}\ddot{\mathbf{q}}(t) + \mathbf{C}\dot{\mathbf{q}}(t) + \mathbf{K}_s\mathbf{q}(t) = \mathbf{f}(t), \quad [-\omega^2\mathbf{M} + i\omega\mathbf{C} + \mathbf{K}_s]\tilde{\mathbf{q}}_a(\omega) = \tilde{\mathbf{f}}_a(\omega). \quad (3a,b)$$

When the system is undamped or proportionally damped, one can obtain real eigenvalues (λ_r) and eigenvectors (\mathbf{u}_r) from the following well-known eigenvalue problem of the undamped system [23]:

$$\mathbf{K}_s\mathbf{u}_r = \lambda_r\mathbf{M}\mathbf{u}_r, \quad \omega_r^2 = \lambda_r. \quad (4a,b)$$

Forced harmonic responses are then obtained by using the classical normal mode expansion method [23]. One may define \mathbf{C} for the proportionally damped system by employing either the Rayleigh’s model [24] or Caughey’s [25] criterion as follows, where α and β are scalar constants:

$$\mathbf{C} = \alpha\mathbf{M} + \beta\mathbf{K}, \quad \mathbf{C}\mathbf{M}^{-1}\mathbf{K} = \mathbf{K}\mathbf{M}^{-1}\mathbf{C}. \quad (5a,b)$$

When equation (5) is not satisfied, a new eigenvalue problem for the non-proportionally damped system must be formulated in the $2N$ space, as given below. The corresponding eigensolutions ($\tilde{\lambda}_r$ and $\tilde{\mathbf{w}}_r$) are complex valued [26, 27]:

$$\mathbf{A}\dot{\mathbf{y}}(t) + \mathbf{B}\mathbf{y}(t) = \mathbf{g}(t), \quad \mathbf{y}(t) = [\dot{\mathbf{q}}(t) \ \mathbf{q}(t)]^T, \quad \mathbf{g}(t) = [\mathbf{0} \ \mathbf{f}(t)]^T, \quad (6a-c)$$

$$\mathbf{A} = \begin{bmatrix} \mathbf{0} & \mathbf{M} \\ \mathbf{M} & \mathbf{C} \end{bmatrix}, \quad \mathbf{B} = \begin{bmatrix} -\mathbf{M} & \mathbf{0} \\ \mathbf{0} & \mathbf{K}_s \end{bmatrix}. \quad (6d,e)$$

Forced harmonic responses of a non-proportionally damped system can also be obtained by using the generalized modal superposition method [26–28]. Basic steps include

$$[i\omega\mathbf{A} + \mathbf{B}]\tilde{\mathbf{y}}_a(\omega) = \tilde{\mathbf{g}}_a(\omega), \quad \tilde{\mathbf{y}}_a(\omega) = [i\omega\tilde{\mathbf{q}}_a(\omega) \ \tilde{\mathbf{q}}_a(\omega)]^T, \quad (7a,b)$$

$$\tilde{\mathbf{g}}_a(\omega) = [\mathbf{0} \ \tilde{\mathbf{f}}_a(\omega)]^T, \quad \mathbf{B}\tilde{\mathbf{w}}_r + \tilde{\lambda}_r\mathbf{A}\tilde{\mathbf{w}}_r = \mathbf{0}, \quad \tilde{\mathbf{w}}_r = [\tilde{\lambda}_r\tilde{\mathbf{u}}_r \ \tilde{\mathbf{u}}_r]^T. \quad (7c-e)$$

First, obtain the normal modal matrix $\tilde{\mathbf{W}}$ from $\tilde{\mathbf{w}}_r$ by solving equation (7d) and then calculate for the modal responses $\tilde{p}_{wra}(\omega)$ by uncoupling equation (7a) as follows:

$$\tilde{\mathbf{y}}_a(\omega) = \tilde{\mathbf{W}}\tilde{\mathbf{p}}_{wa}(\omega), \quad (8a)$$

$$\tilde{\mathbf{p}}_{wa}(\omega) = [\tilde{p}_{w1a}(\omega) \ \cdots \ \tilde{p}_{wra}(\omega) \ \cdots \ \tilde{p}_{w2Na}(\omega)]^T, \quad \tilde{p}_{wra}(\omega) = \frac{\tilde{\mathbf{w}}_r^T \tilde{\mathbf{g}}_a(\omega)}{i\omega - \tilde{\lambda}_r}. \quad (8b,c)$$

3.2.2. *LTI visco-elastic damping models*

For the visco-elastic materials, the dynamic stiffness matrix ($\tilde{\mathbf{K}}_d$) is usually expressed as follows to account for both elastic and dissipative properties: $\tilde{\mathbf{K}}_d = \mathbf{K}'_d + i\mathbf{K}''_d$. Assume that $\mathbf{K}'_d \neq \mathbf{K}'_d(\omega)$ and $\mathbf{K}''_d \neq \mathbf{K}''_d(\omega)$. The governing frequency response equations for a system of dimension N are

$$[-\omega^2\mathbf{M} + \tilde{\mathbf{K}}_d]\tilde{\mathbf{q}}_a(\omega) = \tilde{\mathbf{f}}_a(\omega), \quad \mathbf{D}(\omega)\tilde{\mathbf{q}}_a(\omega) = \tilde{\mathbf{f}}_a(\omega), \quad \tilde{\mathbf{q}}_a(\omega) = \mathbf{D}^{-1}(\omega)\tilde{\mathbf{f}}_a(\omega), \quad (9a-c)$$

$$\mathbf{D}(\omega) = -\omega^2\mathbf{M} + \tilde{\mathbf{K}}_d = -\omega^2\mathbf{M} + \mathbf{K}'_d + i\mathbf{K}''_d. \quad (9d)$$

First, assume that the system is proportionally damped such that $\mathbf{K}''_d = \eta\mathbf{K}'_d$, where the loss factor η is a spectrally invariant scalar constant. Now define an eigenvalue problem by expressing $\mathbf{q}(t) = \mathbf{u}e^{i\omega t}$ for the undamped ($\mathbf{K}''_d = 0$) and unforced ($\tilde{\mathbf{f}}_a(\omega) = 0$) system in equation (9a). This yields an equation like equation (4) where \mathbf{K}_s is replaced by \mathbf{K}'_d . The real eigenvector \mathbf{u} , must satisfy the orthogonal relations with respect to \mathbf{M} and \mathbf{K}'_d [25]. Second, consider the case when this system is non-proportionally damped. Now employ the complex-valued terms $\tilde{\omega}_r$, $\tilde{\lambda}_r$, $\tilde{\mathbf{u}}_r$, and $\tilde{\mathbf{K}}_d$ and rewrite equation (4) as follows:

$$\tilde{\mathbf{K}}_d\tilde{\mathbf{u}}_r = \tilde{\lambda}_r\mathbf{M}\tilde{\mathbf{u}}_r, \quad \tilde{\lambda}_r = \lambda_{rR} + i\lambda_{rI} = \tilde{\omega}_r^2, \quad \tilde{\omega}_r = \omega_{rR} + i\omega_{rI}, \quad (10a-c)$$

$$\omega_{rR} = \sqrt{\frac{\lambda_{rR} + \sqrt{\lambda_{rR}^2 + \lambda_{rI}^2}}{2}}, \quad \omega_{rI} = \sqrt{\frac{-\lambda_{rR} + \sqrt{\lambda_{rR}^2 + \lambda_{rI}^2}}{2}}. \quad (10d,e)$$

Kung and Singh [29] have utilized this eigenvalue formulation for damped beams and found excellent correlations with modal experiments. Unlike the non-proportional viscous damping case given by equations (6) and (7), the complex eigenvalue problem of equation (10) does not need to be transformed into the $2N$ -dimensional space. Also note that eigenvectors $\tilde{\mathbf{u}}_r$ still satisfy the following orthogonal relationship:

$$\tilde{\mathbf{u}}_r^T\mathbf{M}\tilde{\mathbf{u}}_j = \delta_{rj}, \quad \tilde{\mathbf{u}}_r^T\tilde{\mathbf{K}}_d\tilde{\mathbf{u}}_j = \tilde{\lambda}_r\delta_{rj}, \quad r, j = 1, \dots, N, \quad (11a,b)$$

where δ_{rj} is the Kronecker delta function. Note that the transpose of $\tilde{\mathbf{u}}_r$ is taken here instead of employing the Hermitian eigenvector ($\tilde{\mathbf{u}}_r^H$), that is used for the orthogonal relationships for an undamped system given by equation (4), i.e., $\tilde{\mathbf{u}}_r^H\mathbf{M}\tilde{\mathbf{u}}_j^H = \delta_{rj}$. Using the orthogonal properties as given by equation (11) and the normal modal matrix $\tilde{\mathbf{U}}$, the harmonic response amplitude vector $\tilde{\mathbf{q}}_a(\omega)$ is obtained by the modal superposition method,

$$\tilde{\mathbf{q}}_a(\omega) = \tilde{\mathbf{U}}\tilde{\mathbf{p}}_a(\omega), \quad (12)$$

where $\tilde{\mathbf{p}}_a(\omega)$ is the response in modal co-ordinates. Equations (9c) and (12) should yield identical answers unless modal truncation errors are present.

3.2.3. *Combination of viscous and visco-elastic damping models*

When both viscous and visco-elastic damping elements are present within a system, the equations of motion must be expressed only in the ω domain as

$$[-\omega^2\mathbf{M} + i\omega\mathbf{C} + \mathbf{K}_s + \mathbf{K}'_d + i\mathbf{K}''_d]\tilde{\mathbf{q}}_a(\omega) = \tilde{\mathbf{f}}_a(\omega). \quad (13)$$

Four approximate methods will be proposed in this article in order to solve equation (13). First, consider the Type I model that consists of both Rayleigh’s viscous damping model of equation (5a) and the visco-elastic material model ($\mathbf{K}'_d = \eta\mathbf{K}'_d$) where η is scalar. Assume that $\mathbf{K}_s = \Gamma_{sd}\mathbf{K}'_d$, where Γ_{sd} may be called as a scaling factor that relates static and dynamic storage stiffnesses. Such a combined model should yield real eigensolutions based on the eigenvalue problem

$$(\mathbf{K}_s + \mathbf{K}'_d)\mathbf{u}_r = \lambda_r\mathbf{M}_r, \quad (1 + \Gamma_{sd})\mathbf{K}'_d\mathbf{u}_r = \lambda_r\mathbf{M}\mathbf{u}_r. \tag{14a,b}$$

Transforming equation (13) into the modal domain by using \mathbf{u}_r from equation (14), one can obtain the modal response as

$$\tilde{p}_{ra}(\omega) = \frac{\mathbf{u}_r^T \tilde{\mathbf{f}}_a(\omega)}{\omega_r^2 - \omega^2 + i[\alpha\omega + \omega_r^2(\eta + \beta\Gamma_{sd}\omega)]/(1 + \Gamma_{sd})}. \tag{15}$$

Forced harmonic responses are then obtained by using equation (12). Note that normal modal matrix \mathbf{U} is real-valued in this case.

The next three models, designated as Type II, III, and IV models, assume that $\mathbf{K}_s \neq \Gamma_{sd}\mathbf{K}'_d$. Since the eigenvectors from equation (14) do not uncouple equation (13), the eigenvalue problem must include damping terms. This will result in a non-linear eigenvalue problem; such problems will be discussed in the next section. To avoid the non-linear eigenvalue problem, one may instead approximate eigensolutions by using equation (14) and calculate the forced harmonic response by neglecting the off-diagonal terms after the transformation of equation (13) into the modal domain. The model that uses this approach will be called Type II. One may also convert the viscous damping model to visco-elastic damping model by assuming the Voigt (or comparable) model. The contribution of \mathbf{C} , when converted into the visco-elastic damping model, is defined here as \mathbf{K}''_{Cd} . The resulting equivalent (or approximate) equations of motion for Type III model would be

$$[-\omega^2\mathbf{M} + \mathbf{K}'_{de} + i\mathbf{K}''_{de}]\tilde{\mathbf{q}}_a(\omega) = \tilde{\mathbf{f}}_a(\omega), \quad \mathbf{K}'_{de} = \mathbf{K}_s + \mathbf{K}'_d, \quad \mathbf{K}''_{de} = \mathbf{K}''_d + \mathbf{K}''_{Cd}. \tag{16a-c}$$

The eigenvalue problem of equation (16a) is constructed by replacing \mathbf{K}_d with $\mathbf{K}'_{de} + i\mathbf{K}''_{de}$ in equation (10a) and forced harmonic responses are obtained by using equations (16a), (12), and corresponding eigensolutions. The \mathbf{K}''_{Cd} matrix is obtained as follows. Neglect visco-elastic terms of equation (13) and solve equation (4) to obtain ω_r and the normal modal matrix \mathbf{U}_s . Then calculate the modal damping ratios $\zeta_r = (\alpha/\omega_r + \beta\omega_r)/2$. The equivalent loss factor η_{er} is now calculated by using $\eta_{er} = 2\zeta_r$. Construct \mathbf{K}''_{Cd} as follows:

$$\mathbf{K}''_{Cd} = (\mathbf{U}_s^T)^{-1} \begin{bmatrix} \cdot & & \\ & \eta_{er}\omega_r^2 & \\ & & \cdot & \\ & & & \cdot & \\ & & & & \cdot \end{bmatrix} \mathbf{U}_s^{-1}. \tag{17}$$

Similarly, one may convert the visco-elastic damping \mathbf{K}'_d into the viscous damping model where its contribution is defined as $\mathbf{C}_{K'_d}$. The resulting equations for Model IV are

$$[-\omega^2\mathbf{M} + i\omega\mathbf{C}_e + \mathbf{K}_{se}]\tilde{\mathbf{q}}_a(\omega) = \tilde{\mathbf{f}}_a(\omega), \quad \mathbf{C}_e = \mathbf{C} + \mathbf{C}_{K'_d}, \quad \mathbf{K}_{se} = \mathbf{K}_s + \mathbf{K}'_d, \tag{18a-c}$$

$$\mathbf{C}_{K'_d} = (\mathbf{U}'_d)^{-1} \begin{bmatrix} \cdot & & \\ & 2\zeta_{er}\omega_r & \\ & & \cdot & \\ & & & \cdot & \\ & & & & \cdot \end{bmatrix} \mathbf{U}'_d^{-1}. \tag{18d}$$

In equation (18d), $\zeta_{er} = \eta_r/2$ and ω_r and \mathbf{U}_d are obtained by solving equation (4). Note that \mathbf{K}_s should be replaced by \mathbf{K}'_d . For the Type IV model, the eigenvalue problem of equation (18a) becomes equation (7d) when \mathbf{C} and \mathbf{K}_s are replaced by \mathbf{C}_e and \mathbf{K}_{se} , respectively. Using equations (7a) and (8), forced harmonic responses are calculated.

To assess the validity of approximations associated with Type II, III and IV models, one may define several criteria. For example, the error $\varepsilon_{q_j}(\omega)$ will show how the approximate solutions $\hat{q}_{ja}(\omega)$ differ from the exact $\tilde{q}_{ja}(\omega)$ solutions at any ω . One could also obtain a spectrally averaged value $\langle \varepsilon(\omega) \rangle_\omega$ given N_ω frequency points:

$$\varepsilon_{q_j}(\omega) = \frac{|\hat{q}_{ja}(\omega) - \tilde{q}_{ja}(\omega)|}{|\tilde{q}_{ja}(\omega)|}, \quad \langle \varepsilon(\omega) \rangle_\omega = \frac{1}{N_\omega} \sum_{k=0}^{N_\omega-1} \varepsilon(\omega_k). \tag{19a,b}$$

3.3. EXAMPLES

All four models of the previous section will be numerically examined through the machinery isolation system of Figure 3 that includes both viscous and visco-elastic elements. One may easily evaluate frequency response functions using equation (9c). The first example, with parameters of Table 2, considers a non-proportional visco-elastically damped system. The resulting eigensolutions are $\tilde{\mathbf{u}}_1 = [0.0929 - 0.0004i \ 0.0262 + 0.0008i]^T$ at $\tilde{\omega}_1 = 11.1 + 0.83i$ Hz and $\tilde{\mathbf{u}}_2 = [-0.0371 - 0.0011i \ 0.0657 - 0.0003i]^T$ at $\tilde{\omega}_2 = 18.3 + 1.5i$ Hz. These do satisfy equation (11). Further, harmonic responses using equation (12) exactly match with the exact ones given by equation (9c). The second example examines Type I model with parameters that are listed in Table 2. The results are $\mathbf{u}_1 = [0.0929 \ 0.0261]^T$ at $\omega_1 = 13.6$ Hz and $\mathbf{u}_2 = [-0.0369 \ 0.0657]^T$ at $\omega_2 = 22.3$ Hz. Again the modal superposition method using equation (15) yields the same spectra as the exact one given by equation (9c).

The remaining examples consider Type II, III, and IV models, and their parameters are adjusted by defining $k_{s2} = \Gamma_{sd2} K'_{d2}$. The type I model assumes that $\Gamma_{sd2} = 0.5$ but Γ_{sd2} is varied from 0.1 to 10 for the remaining models. The value of $k_{s2} + K'_{d2}$ is, however, retained to ensure that the undamped system is the same as Type I considered. To see the effect of damping, let $\mathbf{C} = \sigma(\alpha \mathbf{M} + \beta \mathbf{K}_s)$ and $\mathbf{K}''_d = \sigma(\eta \mathbf{K}'_d)$. Damping ratios ζ_r from the viscous

TABLE 2

System parameters for examples of section 3 with reference to Figure 3

$m_1 = 100$ kg, $m_2 = 200$ kg, $K'_{d1} = 200$ N/mm, $K'_{d12} = 400$ N/mm	
Example	Other parameters
First	$K''_{d1} = \eta_1 K'_{d1}$, $K''_{d12} = \eta_{12} K'_{d12}$, $K''_{d2} = \eta_2 K'_{d2}$ $K'_{d2} = 2000$ N/mm, $\eta_1 = 0.1$, $\eta_{12} = 0.2$, $\eta_2 = 0.15$ $k_{s1} = k_{s12} = k_{s2} = c_1 = c_{12} = c_2 = 0$
Second	$\mathbf{C} = \alpha \mathbf{M} + \beta \mathbf{K}_s$, $\mathbf{K}_s = \Gamma_{sd} \mathbf{K}'_d$, $\mathbf{K}''_d = \eta \mathbf{K}'_d$ $K'_{d2} = 2000$ N/mm, $\alpha = 0.5$, $\beta = 10^{-5}$, $\Gamma_{sd} = 0.5$, $\eta = 0.1$
Third to Fifth	$\mathbf{C} = \sigma(\alpha \mathbf{M} + \beta \mathbf{K}_s)$, $\mathbf{K}''_d = \sigma(\eta \mathbf{K}'_d)$, $k_{s1} = \Gamma_{sd} K'_{d1}$, $k_{s12} = \Gamma_{sd} K'_{d12}$, $k_{s2} = \Gamma_{sd2} K'_{d2}$, $k_{s2} + K'_{d2} = 3000$ N/mm $\Gamma_{sd} = 0.5$, $\Gamma_{sd2} = 0.1 \sim 10$, $\alpha = 0.5$, $\beta = 10^{-5}$, $\eta = 0.01$, $\sigma = 1, 10$, or 100

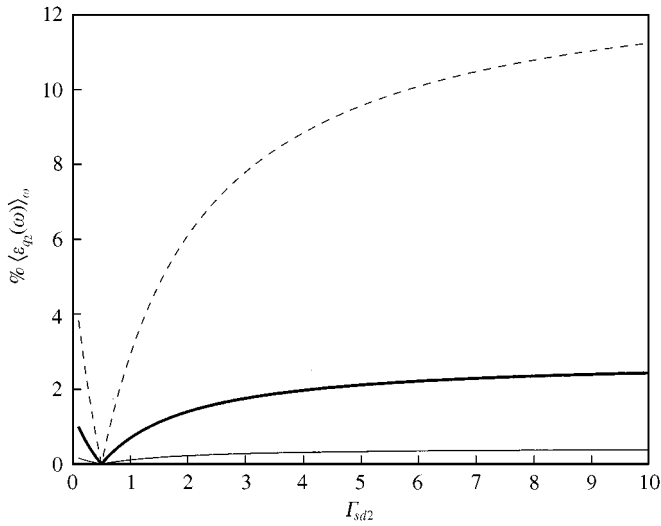


Figure 5. Error introduced by Type II model in the third example of Table 2: —, $\sigma = 1$; — —, $\sigma = 10$; - - -, $\sigma = 100$.

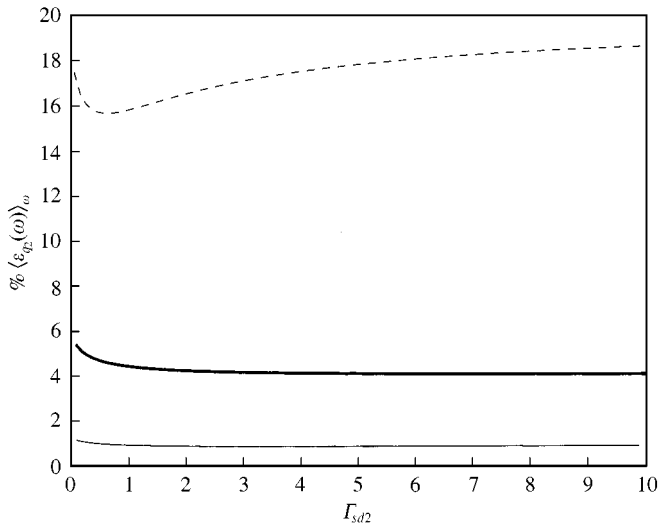


Figure 6. Error introduced by Type III model in the fourth example of Table 2: —, $\sigma = 1$; — —, $\sigma = 10$; - - -, $\sigma = 100$.

damping model range from 0.27 to 0.73% for $\sigma = 1$ (lightly damped), 2.7 to 7.3% for $\sigma = 10$ (moderately damped), and 27 to 73% for $\sigma = 100$ (heavily damped). The results for the Type II model are shown in Figure 5. When $\Gamma_{sd2} = 0.5$, $\langle \varepsilon_{q_2}(\omega) \rangle_\omega$ is zero as expected. But this approximation produces a rather large error for a heavily damped system. Yet it gives good results especially when Γ_{sd2} is from 0.1 to 1.5 since $\langle \varepsilon_{q_2}(\omega) \rangle_\omega$ is less than 5%.

Figure 6 show the results for the Type III model. Even for $\Gamma_{sd2} = 0.5$, $\langle \varepsilon_{q_2}(\omega) \rangle_\omega$ has non-zero values. In addition, overall errors are larger than those observed with the Type II model. To understand this, eigensolutions from both models are compared with the exact

TABLE 3

Comparison of eigensolutions for section 3 examples when $\beta_{sd2} = 0.1$ and $\sigma = 100$

Mode	Model type	Natural frequency $\tilde{\omega}_r$ (Hz)	Eigenvector $\tilde{\mathbf{u}}_r$
1	II	13.6	$[1 \ 0.28]^T$
	III	$15.0 + 6.38i$	$[1 \ 0.26 - 0.018i]^T$
	Exact eigensolution	$13.9 + 8.98i$	$[1 \ 0.24 - 0.038i]^T$
2	II	22.3	$[-0.56 \ 1]^T$
	III	$24.5 + 10.0i$	$[-0.53 + 0.027i \ 1 + 0.017i]^T$
	Exact eigensolution	$23.6 + 13.0i$	$[-0.49 + 0.054i \ 1 + 0.030i]^T$

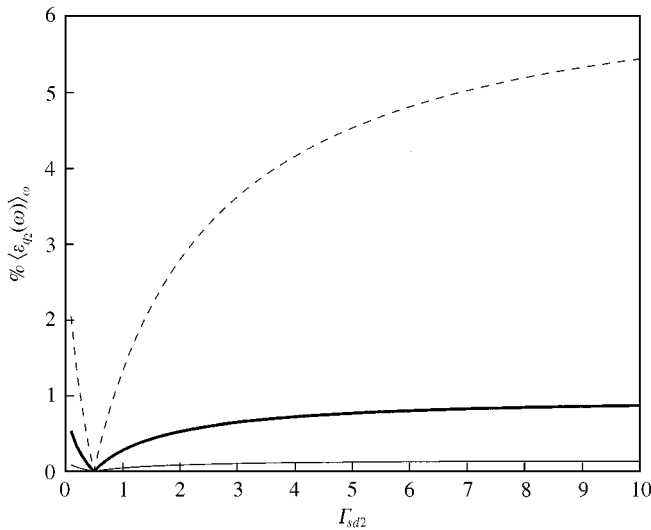


Figure 7. Error introduced by Type III model when equation (13) is used for the uncoupling procedure in the modal superposition method: —, $\sigma = 1$; — —, $\sigma = 10$; - - -, $\sigma = 100$.

solutions which are obtained from the non-linear eigenvalue problem that is described in the next section. However, Table 3 shows that the Type III model better approximates eigensolutions than the Type II model does. This is due to the fact that equation (16a) is used for the uncoupling procedure in the modal superposition method which is an approximate version of equation (13), while the Type II model directly uses equation (13). Figure 7 confirms this finding when the Type III model employs equation (13) instead of equation (16a) based on the modal superposition method. Again for $\Gamma_{sd2} = 0.5$, $\langle \varepsilon_{q_2}(\omega) \rangle_{\omega}$ is zero. Overall errors are about half of those observed for the Type II model.

Next, consider the Type IV model for the final example of Table 2. Results of Figure 8 indicate that the Type IV model predicts results comparable to those from the Type III model (see Figure 6). However, when the values of α and β are decreased by 50%, the Type III model performs much better as shown in Figure 9. Therefore, one may conclude that the Type III model is better suited as an approximation when the visco-elastic damping is more dominant than the viscous damping in a physical system; the Type IV model is recommended for the opposite case.

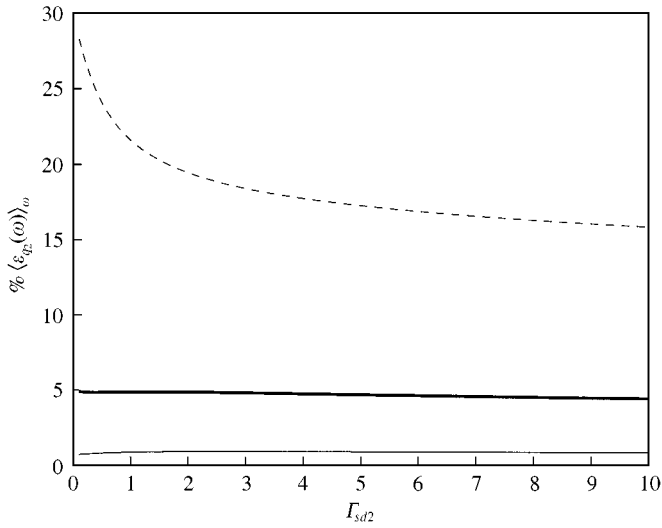


Figure 8. Error introduced by Type IV model in the fifth example of Table 2: —, $\sigma = 1$; — —, $\sigma = 10$; ···, $\sigma = 100$.

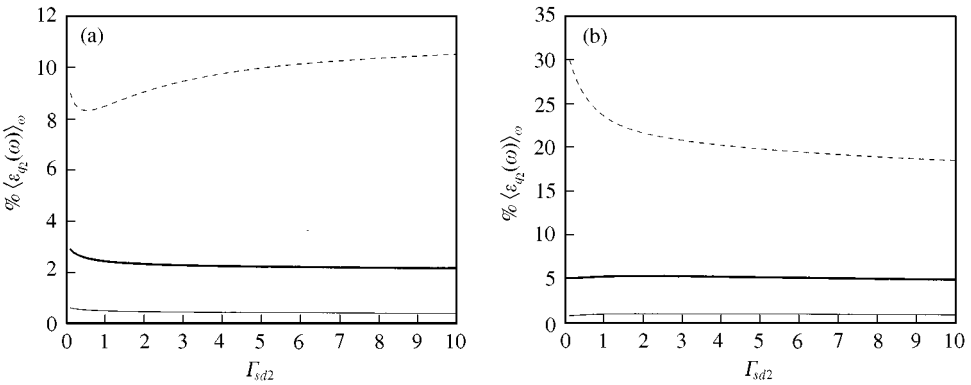


Figure 9. Errors associated with (a) Type III and (b) Type IV models when the viscous damping parameters (α and β) are reduced by 50%: —, $\sigma = 1$; — —, $\sigma = 10$; ···, $\sigma = 100$.

4. EXAMINATION OF PROBLEMS WITH SPECTRALLY VARYING PROPERTIES

4.1. LITERATURE REVIEW

Lumped parameter Voigt, Maxwell, or Burgers type models are often suggested to simulate the measured spectral properties employed to describe the dynamics of visco-elastic materials [9, 14]. For instance, Gaillard and Singh [20] have proposed several linear and non-linear models of automotive clutches that include both visco-elastic and dry friction elements. Predictions compare reasonably well with limited torsional vibration data even though the physical mechanisms are yet to be understood.

The frequency-dependent properties lead to a non-linear eigenvalue problem. Lin and Lim [30] have proposed a perturbation method that is used to find η of damping materials. Similarly, Kung and Singh [29] have assumed spectrally invariant loss factors only within certain frequency bands (say around the natural frequencies). Their formulations have been

successful in describing the modal behavior of beam and plates with multiple damping patches. Przemieniecki [31] has developed frequency-dependent mass and stiffness matrices in the finite element method (FEM) to improve accuracy and reduce the computations required to estimate natural frequencies and mode shapes of continuous linear elastic systems. Note that the frequency-dependent properties in FEM type problems arise due to the numerical discretization of the spectrally invariant continuous elastic structure, not from stiffness or damping element properties. Fergusson and Pilkey [17] have found relationships between the coefficients in the power series expansions for several types of structural matrices, facilitating a more systematic approach in using frequency-dependent structural matrices for FEM formulations. Recently, Brilla [32] has attempted to establish orthogonal properties for approximate eigensolutions using the Laplace transform method for visco-elastic problems. However, the fundamental properties of frequency-dependent visco-elastic materials are yet to be understood.

4.2. ANALYTICAL FORMULATION

The perturbation type approaches are obviously not applicable to hydraulic mounts and similar devices since their dynamic properties may vary significantly over the applicable range. For example, the stiffness modulus $|\tilde{\mathbf{K}}_d|$ of a typical hydraulic engine mount could vary substantially, depending on ω or X as evident from Figure 2. Another key characteristics of dynamic system with frequency dependent-stiffness is that in general the modal superposition method is not valid since the eigenvectors do not follow the conventional orthogonal relations [30]. This aspect alone produces some challenge in predicting the forced response of frequency-dependent structures using the experimentally measured modes. The feasibility of using the modal superposition method will be investigated for such a problem and the associated errors will be assessed to suggest some guidelines. For example, the method may be acceptable when the error is within 10%.

4.2.1. Non-linear eigenvalue problem

For a system with frequency-dependent visco-elastic stiffnesses, use the same governing equations as equation (9a) except now replace $\tilde{\mathbf{K}}_d$ with $\tilde{\mathbf{K}}_d(\omega)$. This yields a non-linear eigenvalue problem that can be seen from equation (10a) when $\tilde{\mathbf{K}}_d$ is replaced by $\tilde{\mathbf{K}}_d(\omega_R)$.

Rewrite them as follows:

$$[-\omega^2 \mathbf{M} + \tilde{\mathbf{K}}_d(\omega)] \tilde{\mathbf{q}}_a(\omega) = \tilde{\mathbf{f}}_a(\omega), \quad \tilde{\mathbf{K}}_d(\omega, R) \tilde{\mathbf{u}}_r = \tilde{\lambda}_r \mathbf{M} \tilde{\mathbf{u}}_r. \quad (20a,b)$$

As a special case, consider the following type of stiffness matrix:

$$\tilde{\mathbf{K}}_d = \tilde{a}(\omega) \tilde{\mathbf{K}}_{do}, \quad \tilde{\mathbf{K}}_{do} = \tilde{\mathbf{K}}_d(\omega_o), \quad (21a,b)$$

where $\tilde{a}(\omega)$ is scalar and a function of ω and $\tilde{\mathbf{K}}_d(\omega_o)$ is evaluated at a reference frequency ω_o . Substitute equation (21a) into equation (20b) and obtain

$$\tilde{\mathbf{K}}_{do} \tilde{\mathbf{u}}_r = \frac{\tilde{\lambda}_r}{\tilde{a}(\omega, R)} \mathbf{M} \tilde{\mathbf{u}}_r. \quad (22)$$

Hence, the frequency dependency affects only the eigenvalues while maintaining the same eigenvectors as those given by $\tilde{\mathbf{K}}_{do} \tilde{\mathbf{u}}_r = \tilde{\lambda}_r \mathbf{M} \tilde{\mathbf{u}}_r$. Here, $\tilde{\mathbf{u}}_r$ satisfies the orthogonal relations given by equation (11). However, for the general case of $\tilde{\mathbf{K}}_d = \tilde{\mathbf{K}}_d(\omega)$ the resulting eigen-vectors

$\tilde{\mathbf{u}}_r$ from equation (20b) may not exhibit the orthogonality properties with respect to the \mathbf{M} or $\tilde{\mathbf{K}}_d(\omega)$ matrices.

Since equation (20) is non-linear, it is difficult to determine the number of eigenvalues it may have even though the dimension of \mathbf{M} or $\tilde{\mathbf{K}}_d(\omega)$ is N . When the number of eigenvalues of equation (20b) exceeds the system dimension N , one should observe more than N peaks in the dynamic compliance spectra for a lightly damped system. For example, consider the case when the mount system is modelled by a single-d.o.f. oscillator; the number of peaks depends on the characteristics of the measured dynamic stiffness, which itself may exhibit multi-dimensional behavior due to its frequency dependence. Singh *et al.* [10] have observed it in their transmissibility studies based on measured mount data.

Based on the discussions presented in this and the previous sections, various eigenvalue problems may be classified depending on the visco-elastic damping formulation. Table 4 summarizes such a classification.

4.2.2. Forced harmonic responses

When the system dimension N is relatively small, forced harmonic responses can be easily calculated by using

$$\tilde{\mathbf{q}}_a(\omega) = \mathbf{D}^{-1}(\omega)\tilde{\mathbf{f}}_a(\omega), \quad \mathbf{D}(\omega) = -\omega^2\mathbf{M} + \tilde{\mathbf{K}}_d(\omega) = -\omega^2\mathbf{M} + \mathbf{K}'_d(\omega) + i\mathbf{K}''_d(\omega). \quad (23a,b)$$

A look-up table may be used to find $\tilde{\mathbf{K}}_d(\omega)$ values, and the responses are calculated at one frequency at a time. However, this calculation procedure is not cost-effective when N becomes rather large, for example when this calculation is attempted with a FEM type numerical code. Therefore, the modal expansion technique should be adopted as the first calculation method. Since the modal superposition method requires that eigenvectors must satisfy equation (11), this approximation implies that $\tilde{\mathbf{u}}_r$ as obtained from equation (20b) is assumed to be orthogonal with respect to the \mathbf{M} and $\tilde{\mathbf{K}}_d(\omega)$ matrices. Therefore, equation (11) must be employed to examine the validity of the orthogonality condition. Note here that only N distinct eigenvalues and eigenvectors are assumed to exist. The following error (ε_1^2) criterion may be proposed to assess the extent of deviation from the orthogonality property:

$$\varepsilon_1^2(\omega) = \frac{|\det[\text{diag}(\tilde{\mathbf{M}}_M)]| - |\det[\tilde{\mathbf{M}}_M]|}{|\det[\tilde{\mathbf{M}}_M]|} + \frac{|\det[\text{diag}(\tilde{\mathbf{K}}_{dM}(\omega))]| - |\det[\tilde{\mathbf{K}}_{dM}(\omega)]|}{|\det[\tilde{\mathbf{K}}_{dM}(\omega)]|}, \quad (24a)$$

$$\tilde{\mathbf{M}}_M = \tilde{\mathbf{U}}^T\mathbf{M}\tilde{\mathbf{U}}, \quad \tilde{\mathbf{K}}_{dM}(\omega) = \tilde{\mathbf{U}}^T\tilde{\mathbf{K}}_d(\omega)\tilde{\mathbf{U}}, \quad (24b,c)$$

where $\tilde{\mathbf{U}}$ is the modal matrix corresponding to equation (20b) and the subscript M denotes the modal domain. When ε_1^2 is small, we may apply the modal expansion method, given by equation (12), to approximate the forced harmonic response.

Two approximate methods are considered next. One may first assume $\tilde{\mathbf{K}}_d$ to contain elements with constant values that are evaluated at ω_o . Now use any LTI method such as equation (12); this will be called the approximate Method I. In the approximate Method II, assume that only N eigenvalues and eigenvectors result from equation (20b), and further assume the solution to be of the form of equation (12). Pre-multiply both sides of equation (20a) by $\tilde{\mathbf{U}}^T$ and obtain

$$[-\omega^2\tilde{\mathbf{M}}_M + \tilde{\mathbf{K}}_{dM}(\omega)]\tilde{\mathbf{p}}_a(\omega) = \tilde{\mathbf{U}}^T\tilde{\mathbf{f}}_a(\omega). \quad (25)$$

TABLE 4
Classification of eigenvalue problems depending on damping model

Damping model	Mathematical representation	Eigenvalue problem (Dimension)	Eigenvalues (number of eigenvalues)	Eigen-vectors	Orthogonality
Viscous, proportional	$\mathbf{C} = \alpha\mathbf{M} + \beta\mathbf{K}_s$	$\mathbf{K}_s\mathbf{u}_r = \lambda_r\mathbf{M}\mathbf{u}_r$	(N) Real (N)	Real	Valid
Viscous, non-proportional	$\mathbf{C} \neq \alpha\mathbf{M} + \beta\mathbf{K}_s$	$\mathbf{B}\tilde{\mathbf{w}}_r = \tilde{\lambda}_r\mathbf{A}\tilde{\mathbf{w}}_r$	(2N) Complex (2N)	Complex	Valid
		$\mathbf{A} = \begin{bmatrix} \mathbf{0} & \mathbf{M} \\ \mathbf{M} & \mathbf{C} \end{bmatrix};$ $\mathbf{B} = \begin{bmatrix} -\mathbf{M} & \mathbf{0} \\ \mathbf{0} & \mathbf{K}_s \end{bmatrix};$ $\tilde{\mathbf{w}}_r = \begin{bmatrix} \tilde{\lambda}_r\tilde{\mathbf{u}}_r \\ \tilde{\mathbf{u}}_r \end{bmatrix}$			
Visco-elastic, proportional	$\tilde{\mathbf{K}}_d = \mathbf{K}'_d(1 + i\eta)$	$\mathbf{K}'_d\mathbf{u}_r = \lambda\mathbf{M}\mathbf{u}_r$	(N) Real (N)	Real	Valid
Visco-elastic, non-proportional	$\tilde{\mathbf{K}}_d = \mathbf{K}'_d + i\mathbf{K}''_d$	$\tilde{\mathbf{K}}_d\tilde{\mathbf{u}}_r = \tilde{\lambda}_r\mathbf{M}\tilde{\mathbf{u}}_r$	(N) Complex (N)	Complex	Valid
Visco-elastic, proportionally varying frequency dependent	$\tilde{\mathbf{K}}_d(\omega) = \tilde{a}(\omega)\tilde{\mathbf{K}}_{do}$ $\tilde{\mathbf{K}}_{do} = \tilde{\mathbf{K}}_d(\omega_o)$	$\tilde{\mathbf{K}}_{do}\tilde{\mathbf{u}}_r = \frac{\tilde{\lambda}_r}{\tilde{a}(\omega_R)}\mathbf{M}\tilde{\mathbf{u}}_r$ $\tilde{\omega}_r^2 = \tilde{\lambda}_r; \tilde{\omega}_r = \omega_{rR} + i\omega_{rI}$	(N) Complex (N)	Complex	Valid
Visco-elastic, non-proportionally varying frequency dependent	$\tilde{\mathbf{K}}_d(\omega) \neq \tilde{a}(\omega)\tilde{\mathbf{K}}_{do}$ or $\tilde{\mathbf{K}}_d(\omega) = \mathbf{K}'_d(\omega) + i\mathbf{K}''_d(\omega)$	$\tilde{\mathbf{K}}_d(\omega_R)\tilde{\mathbf{u}}_r = \tilde{\lambda}_r\mathbf{M}\tilde{\mathbf{u}}_r$ $\tilde{\omega}_r^2 = \tilde{\lambda}_r; \tilde{\omega}_r = \omega_{rR} + i\omega_{rI}$	(N) Complex ($\geq N$)	Complex	Invalid

Note: (1) Loss factor η is a spectrally invariant scalar constant. (2) \mathbf{M} , \mathbf{C} , and \mathbf{K}_s are real symmetric matrices. (3) Dynamic stiffness matrix $\tilde{\mathbf{K}}_d$ is not Hermitian, rather it is complex symmetric, i.e., $\tilde{\mathbf{K}}_d = \tilde{\mathbf{K}}_d^t$.

An approximate solution may be obtained by taking only the diagonal terms in the modal domain while neglecting off-diagonal terms as follows:

$$\begin{bmatrix} \cdot & & \\ & m_r & \\ & & \cdot & \cdot \\ & & & \cdot & \cdot \\ & & & & \cdot & \cdot \\ & & & & & \cdot & \cdot \\ & & & & & & \cdot & \cdot \\ & & & & & & & \cdot & \cdot \\ & & & & & & & & \cdot & \cdot \end{bmatrix} = \text{diag} [\mathbf{M}_M], \quad \begin{bmatrix} \cdot & & \\ & \tilde{k}_r(\omega) & \\ & & \cdot & \cdot \\ & & & \cdot & \cdot \\ & & & & \cdot & \cdot \\ & & & & & \cdot & \cdot \\ & & & & & & \cdot & \cdot \\ & & & & & & & \cdot & \cdot \\ & & & & & & & & \cdot & \cdot \end{bmatrix} = \text{diag} [\tilde{\mathbf{K}}_{dM}(\omega)], \quad (26a,b)$$

$$\tilde{p}_{ra}(\omega) = \frac{\tilde{\mathbf{u}}_r^T \tilde{\mathbf{f}}_a}{-\omega^2 m_r + \tilde{k}_r(\omega)}, \quad (26c)$$

where \tilde{p}_{ra} is the r th element of $\tilde{\mathbf{p}}_a$ or the approximate response of the r th modal coordinate. The resulting solution $\hat{\mathbf{q}}_a$ from the modal superposition method, as given by equation (12), is only an estimate of the true solution $\tilde{\mathbf{q}}_a$ that is given by equation (23a). Note that the errors involved in this approximation occur due to the absence of off-diagonal terms of dynamic stiffness ($\mathbf{D}_M(\omega)$) in modal co-ordinates. To assess the associated error, the following error criterion ε_2^2 is defined to measure how close $\text{diag}(\mathbf{D}_M(\omega))$ is to $\mathbf{D}_M(\omega)$; recall that ε_1^2 of equation (24a) is based on the deviation of eigenvectors from the orthogonal properties:

$$\varepsilon_2^2(\omega) = \frac{\|\det[\text{diag}(\mathbf{D}_M(\omega))] - \det[\mathbf{D}_M(\omega)]\|}{\|\det[\mathbf{D}_M(\omega)]\|}, \quad \mathbf{D}_M(\omega) = -\omega^2 \mathbf{M}_M + \tilde{\mathbf{K}}_{dM}(\omega). \quad (27a,b)$$

The following two response-related error criteria are also defined to judge the validity of two approximations that have been proposed here:

$$\varepsilon_3(\omega) = \frac{|\hat{\mathbf{q}}_a(\omega) - \tilde{\mathbf{q}}_a(\omega)|}{|\tilde{\mathbf{q}}_a(\omega)|}, \quad \varepsilon_4(\omega) = \frac{\|\hat{\mathbf{q}}_a(\omega) - \tilde{\mathbf{q}}_a(\omega)\|}{\|\tilde{\mathbf{q}}_a(\omega)\|}. \quad (28a,b)$$

Correlations between ε_1 , ε_2 , ε_3 , and ε_4 will be examined in the next section for selected examples.

4.3. EXAMPLES

The first example considers the Type III model of section 3.2.3. However, in this example, the forced harmonic response will be calculated by using the eigenvectors from the non-linear eigenvalue problem (20b). The resulting errors based on the exact eigenvectors are negligible when σ is varied from 1 to 10. Error grows only when σ is very large, say 100. Compare these to the results of Figure 7 where the approximate eigenvectors of the Type III model are used. Significant improvement is observed even for a heavily damped system.

A comparison between the exact solution (9c) and the modal expansion method (12) is sought when the stiffness type of equation (21) is selected. The parameters of the first example of Table 2 are used here except $\tilde{a}(\omega) = 1 + \omega/(100\pi)$. Since eigenvectors are orthogonal with respect to \mathbf{M} or $\tilde{\mathbf{K}}_d(\omega)$, both solutions yield exactly the same results.

Next, consider some spectrally varying stiffnesses to investigate the effects of their properties. Assume that $\tilde{K}_d(\omega)$ is an analytical function over $\omega_L \leq \omega - \omega_o \leq \omega_H$ with

$$K'_d(\omega) = K'_{do} \left(1 + \sum_{n=1}^{N'} a_n \varpi^n \right), \quad K''_d(\omega) = K''_{do} \left(1 + \sum_{n=1}^{N''} b_n \varpi^n \right), \quad (29a,b)$$

TABLE 5

System parameters for examples of section 4 with reference to Figure 3

Example	Parameters
First	The fourth example of Table 2
Second	The first example of Table 2 and $\tilde{a}(\omega) = 1 + \omega/(100\pi)$
Third to Fifth	$\mathbf{C} = \sigma_s(\alpha\mathbf{M} + \beta\mathbf{K}_s)$, $k_{s1} = \Gamma_{sd}K'_{d1o}$, $k_{s12} = \Gamma_{sd}K'_{d12o}$, $k_{s2} = \Gamma_{sd2}K'_{d2o}$, $K''_{d1o} = \sigma_{d1}\eta_1K'_{d1o}$, $K''_{d12o} = \sigma_{d12}\eta_{12}K'_{d12o}$, $K''_{d2o} = \sigma_{d2}\eta_2K'_{d2o}$, $k_{s2} + K'_{d2o} = 3000$ N/mm, $K'_{d1o} = 200$ N/mm, $K'_{d12o} = 400$ N/mm, $\alpha = 0.5$, $\beta = 10^{-5}$, $m_1 = 100$ kg, $m_2 = 200$ kg
Third to Fourth	$\sigma_s = \sigma_{d1} = \sigma_{d12} = \sigma_{d2} = 1.0$, $\Gamma_{sd} = 0.5$, $\Gamma_{sd2} = 1.0$, $\eta_1 = \eta_{12} = \eta_2 = 0.1$
Third	$N'' = N'$, $b_1 = a_1$, $N' = 1$, $a_1 = 0.1$, 1, or 2
Fourth	$N'' = 1$ vs. $N' = 2$ $N'' = N'$, $b_n = a_n$ $N' = 1$: $a_1 = 0.1$ $N' = 2$: $a_1 = 0.1$ and $a_2 = 0.1$, 1, or 2
	$N'' = 2$ vs. $N' = 3$ $N'' = N'$, $b_n = a_n$ $N' = 2$: $a_1 = 0.1$, $a_2 = 0.1$ $N' = 3$: $a_1 = 0.1$, $a_2 = 0.1$, $a_3 = 0.1$, 1, or 2
Fifth	$N'' = N'$ for $\tilde{K}_{d1}(\omega)$, $\tilde{K}_{d12}(\omega)$, and $\tilde{K}_{d2}(\omega)$ σ_s , σ_{d1} , σ_{d12} , and $\sigma_{d2} = R(1, 100)$, [†] $\beta_{sd2} = R(0.1, 10)$, $\eta_1 = \eta_{12} = \eta_2 = 0.005$
	$N' = 1$ a_1 and $b_1 = R(0.1, 2)$
	$N' = 2$ a_1, a_2, b_1 , and $b_2 = R(0.1, 2)$
	$N' = 3$ a_1, a_2, a_3, b_1, b_2 , and $b_3 = R(0.1, 2)$

[†] $R(a, b)$ = random function that assigns values from a to b .

where $K'_{do} = K'_d(\omega_o)$, $K''_{do} = K''_d(\omega_o)$, and $\varpi = (\omega - \omega_o)/\max(|\omega - \omega_o|)$. Also choose $\omega_o = \omega_L = 0$ Hz, and $\omega_H = 50$ Hz. Other parameters of the system of Figure 3 are listed in Table 5.

The results of the third example are shown in Figure 10 where $|\tilde{H}_{22}(\omega)|$ spectra are compared between the exact solution and approximation I that assumes $\tilde{K}_d = \tilde{K}_{do}$. This approximation gives reasonably good results as long as the stiffness variation is less than 10% over the frequency range.

The fourth example examines the effects of higher orders in equation (29). Comparison between $N' = 1$ and 2 is shown in Figure 11(a). Effects of $N' = 2$ and $N' = 3$ are shown in Figure 11(b). With the same amount of variation, say 10 or 100%, the addition of higher order terms has a reduced effect on the dynamic compliance. Consequently, the approximation I may be used, even over a larger frequency range, provided the range is divided into several regions such that the stiffness variation is less than 10% within each region.

Finally, the approximation II is considered to assess the resulting errors and to examine correlations between error indices based on three stiffness types as listed as the fifth example in Table 5. Given 150 randomly selected sets of parameters, the correlation coefficients γ [33] between spectrally averaged error indices $\langle \varepsilon_1(\omega) \rangle_\omega$, $\langle \varepsilon_2(\omega) \rangle_\omega$, $\langle \varepsilon_3(\omega) \rangle_\omega$, and $\langle \varepsilon_4(\omega) \rangle_\omega$ are calculated from 0 to 50 Hz, as shown in Figures 12–14. One can observe

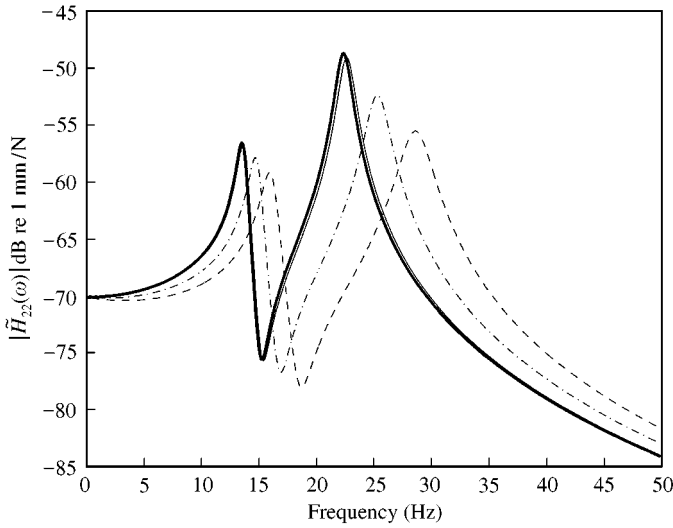


Figure 10. Comparison of dynamic compliance spectra for the third example of Table 5: —, approximation I; —, exact solution for $a_1 = 0.1$; - - -, $a_1 = 1$; - · - · -, $a_1 = 2$.

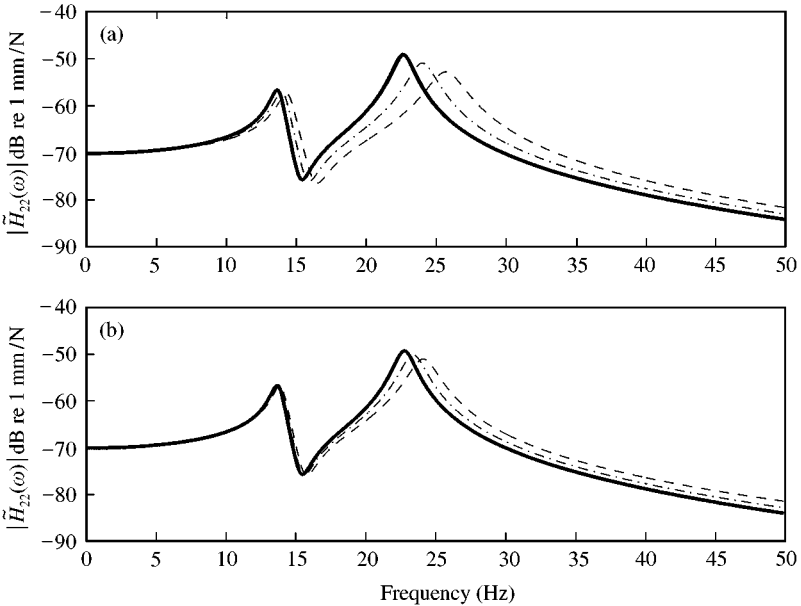


Figure 11. Effect of higher orders of $\tilde{K}_d(\omega)$ on dynamic compliance spectra for the fourth example of Table 5. (a) $N' = 1$ vs. $N' = 2$, (b) $N' = 2$ vs. $N' = 3$. (a) —, $N' = 1$; —, $N' = 2$ ($a_2 = 0.1$); - - -, $N' = 2$ ($a_2 = 1$); - · - · -, $N' = 2$ ($a_2 = 2$) and (b) —, $N' = 2$; —, $N' = 3$ ($a_3 = 0.1$); - - -, $N' = 3$ ($a_3 = 1$); - · - · -, $N' = 3$ ($a_3 = 2$).

that ε_1 is poorly correlated with ε_3 and ε_4 . But ε_3 and ε_4 correlate well with ε_2 . Therefore, one may conclude that the forced harmonic response can be reasonably approximated, with less than 10% error, by the modal expansion method only when $\langle \varepsilon_2(\omega) \rangle_\omega$ is less than 4%.

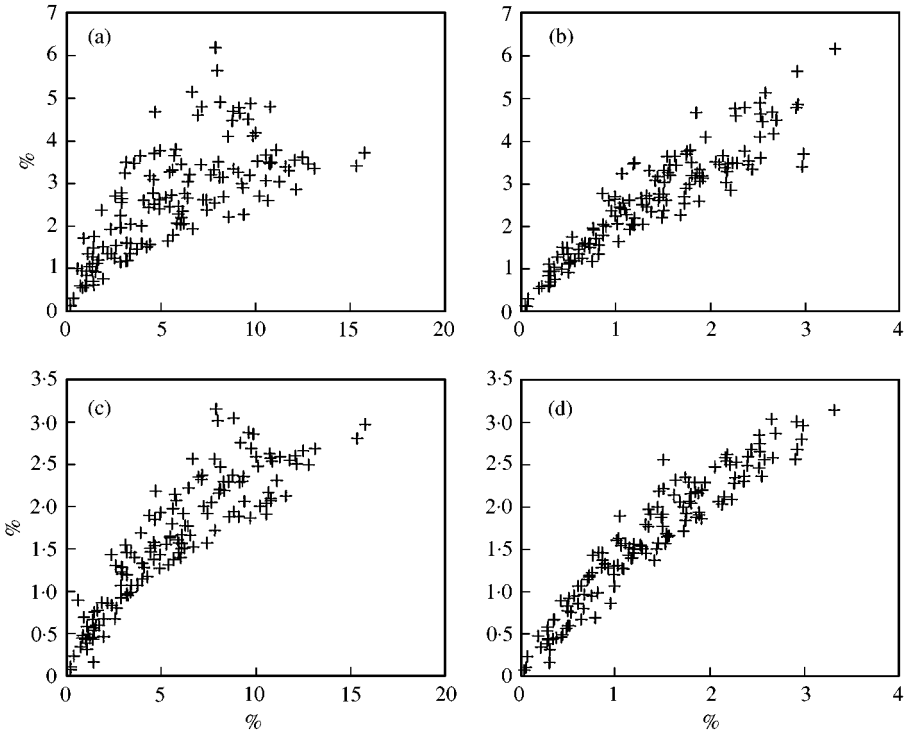


Figure 12. Correlation between error indices for the fifth example ($N' = 1$) of Table 5. (a) $\langle \varepsilon_3 \rangle_\omega$ versus $\langle \varepsilon_1 \rangle_\omega$; $\gamma = 0.71$, (b) $\langle \varepsilon_3 \rangle_\omega$ versus $\langle \varepsilon_2 \rangle_\omega$; $\gamma = 0.92$, (c) $\langle \varepsilon_4 \rangle_\omega$ versus $\langle \varepsilon_1 \rangle_\omega$; $\gamma = 0.89$, (d) $\langle \varepsilon_4 \rangle_\omega$ versus $\langle \varepsilon_2 \rangle_\omega$; $\gamma = 0.96$.

5. QUASI-LINEAR MODEL

5.1. 1/2-CAR MODEL

Kim and Singh [8] developed a quasi-linear method and applied it to a 1/4 car model. Their method has identified superior resonance control characteristics of the hydraulic mount over the rubber mount in the low-frequency regime. Also, it has predicted the well-known poor performance of the passive hydraulic mount at higher frequencies. This quasi-linear method is applied to the 1/2 car model of Figure 4 since this model has not been specifically examined before. Eigensolutions of this system are sought first and then forced harmonic responses are calculated assuming the vehicle is subjected to either engine excitation force or road displacement input. To avoid any non-linearity in the governing equation, $\tilde{\mathbf{K}}_d(\omega, X)$ is evaluated at a given X_o as $\tilde{\mathbf{K}}_d(\omega; X_o)$, which is then used in place of $\tilde{\mathbf{K}}_d(\omega)$ in equation (20a). Equations of motions for Figure 4 can be easily derived, in terms of the generalized displacement vector $\mathbf{q}(t) = [q_1(t) \ q_2(t) \ q_3(t) \ q_4(t) \ q_5(t) \ q_6(t)]^T$ and force vector $\tilde{\mathbf{f}}_a = [F_1 \ 0 \ k_{s3}\tilde{q}_{7a} \ 0 \ 0 \ k_{s6}\tilde{q}_{8a}]^T$. The resulting dynamic stiffness matrix will include $\tilde{\mathbf{K}}_d(\omega; X_o)$ terms.

5.2. RESULTS

The following parameters are chosen for the 1/2 car of Figure 4: $m_1 = 125$ kg, $m_2 = 220$ kg, $m_3 = 45$ kg, $m_4 = 270$ kg, $m_5 = 240$ kg, $m_6 = 75$ kg, $k_{s23} = 22$ N/mm,

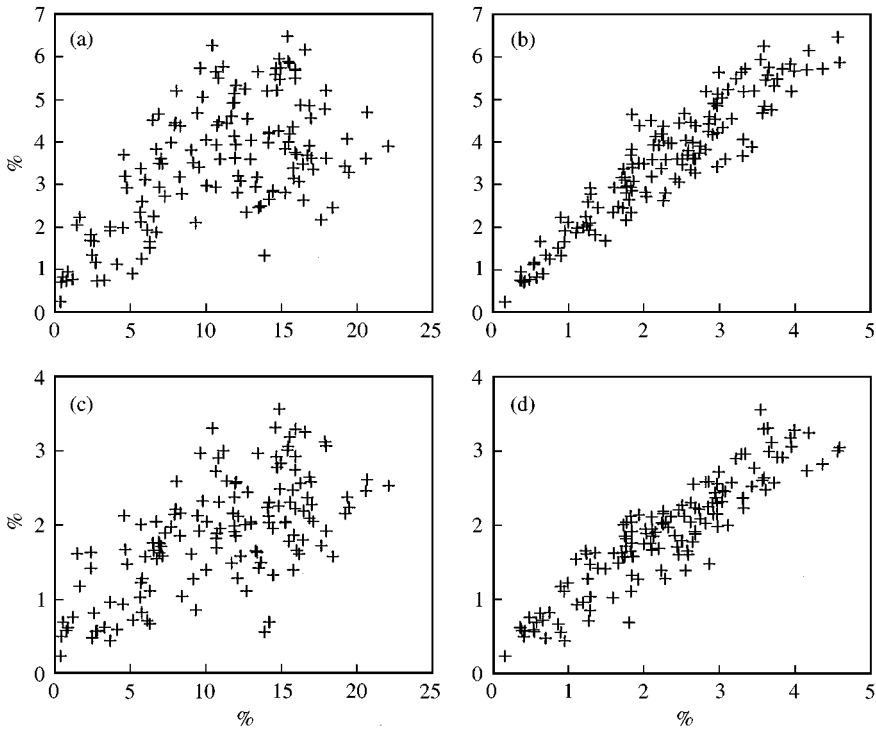


Figure 13. Correlation between error indices for the fifth example ($N' = 2$) of Table 5. (a) $\langle \varepsilon_3 \rangle_\omega$ versus $\langle \varepsilon_1 \rangle_\omega$; $\gamma = 0.59$, (b) $\langle \varepsilon_3 \rangle_\omega$ versus $\langle \varepsilon_2 \rangle_\omega$; $\gamma = 0.93$, (c) $\langle \varepsilon_4 \rangle_\omega$ versus $\langle \varepsilon_1 \rangle_\omega$; $\gamma = 0.65$, (d) $\langle \varepsilon_4 \rangle_\omega$ versus $\langle \varepsilon_2 \rangle_\omega$; $\gamma = 0.91$.

$k_{s24} = 2000$ N/mm, $k_{s3} = 200$ N/mm, $k_{s45} = 1800$ N/mm, $k_{s56} = 26$ N/mm, and $k_{s6} = 200$ N/mm. Measured data for two typical hydraulic mounts (B and C) are shown in Figure 15; note that their properties differ considerably from those of A (Figure 2). Eigenvalues for hydraulic mount B are listed in Table 6; these are solved by using the non-linear eigenvalue problem (20b). The number of eigenvalues (7) is more than the system dimension (6) due to the frequency-dependent mount properties. Examples of frequency response functions are shown in Figure 16 where the effect of X is clearly observed even though the quasi-linear method is employed. Similar analyses may be conducted for any mount, over the given range of measured data. This may yield useful design information.

6. ANALYSIS OF PROBLEMS WITH FREQUENCY- AND AMPLITUDE-DEPENDENT PROPERTIES

6.1. LITERATURE REVIEW

Mathematical models of selected mounts or related phenomena have been attempted which illustrate some of the non-linear mechanisms involved. For example, Kim and Singh [8] have successfully developed a non-linear model of hydraulic engine mounts that requires the measurement of fundamental fluid system parameters. However, the model is device specific, and therefore one must construct a new simulation model from basic principles and laboratory measurements for each component. Such a model, though obtained via a time-consuming process, when available, can be extremely useful. For

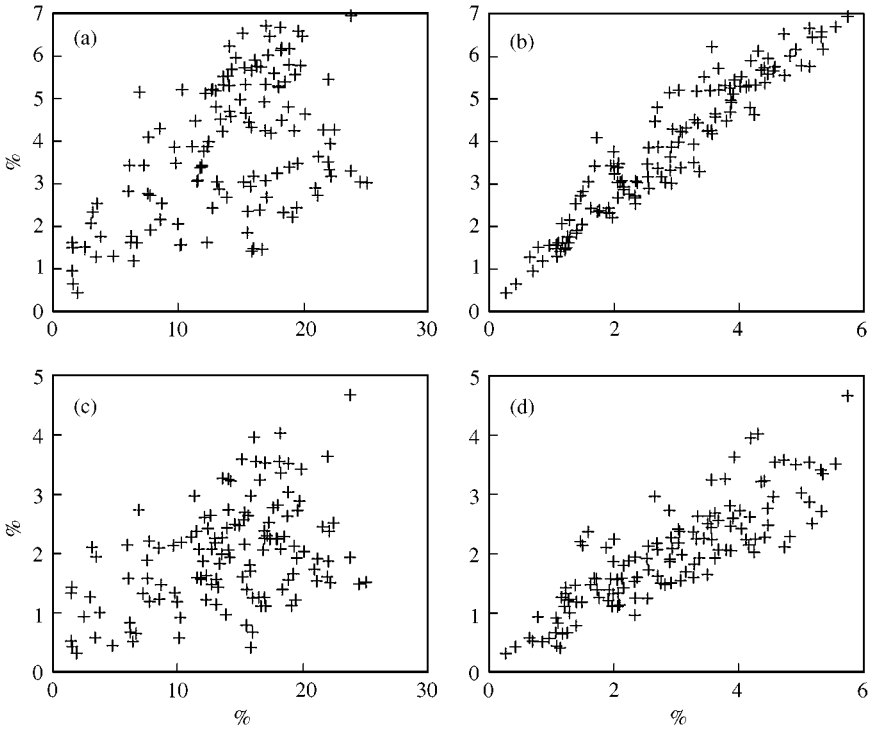


Figure 14. Correlation between error indices for the fifth example ($N = 3$) of Table 5. (a) $\langle \epsilon_3 \rangle_\omega$ versus $\langle \epsilon_1 \rangle_\omega$; $\gamma = 0.51$, (b) $\langle \epsilon_3 \rangle_\omega$ versus $\langle \epsilon_2 \rangle_\omega$; $\gamma = 0.95$, (c) $\langle \epsilon_4 \rangle_\omega$ versus $\langle \epsilon_1 \rangle_\omega$; $\gamma = 0.45$, (d) $\langle \epsilon_4 \rangle_\omega$ versus $\langle \epsilon_2 \rangle_\omega$; $\gamma = 0.85$.

example, Royston and Singh [34, 35] extended the models of Kim and Singh [8] and studied the vibratory energy flow issues.

Several linear system synthesis methods have been developed based on mobility concepts [18, 36] or modal methods [37–39]. The modal techniques suffer in accuracy when only a finite number of vibration modes is used [40, 41]. Some investigators have also included local non-linearities in their synthesis models [42–47]. In particular, Royston and Singh [34] have developed a dual-domain synthesis method for a hydraulic mount, where some non-linearities are handled in the time domain using the enhanced Galerkin method. Non-linearity in the frequency domain is described via a relationship between frequency and dynamic stiffness, but the sub-system itself, as defined in the frequency domain, is still linear.

6.2. NON-LINEAR SYNTHESIS METHOD

The single- or multi-term harmonic balance technique [19, 48], describing function approach [49], or Galerkin methods [34, 35, 50, 51] have been very successful in considering strong non-linearities. Such methods, however, explicitly demand a time domain model that may require considerable effort to develop, given limited measurements as mentioned previously. Instead, it is proposed that the measured $\tilde{K}_d(\omega, X)$ data be directly used in developing a system model. Note that the measured $\tilde{K}_d(\omega, X)$ of a non-linear device exactly corresponds to the single-term harmonic balance technique. One could, however, expand this approach further in future where the ‘black box’ could be characterized using

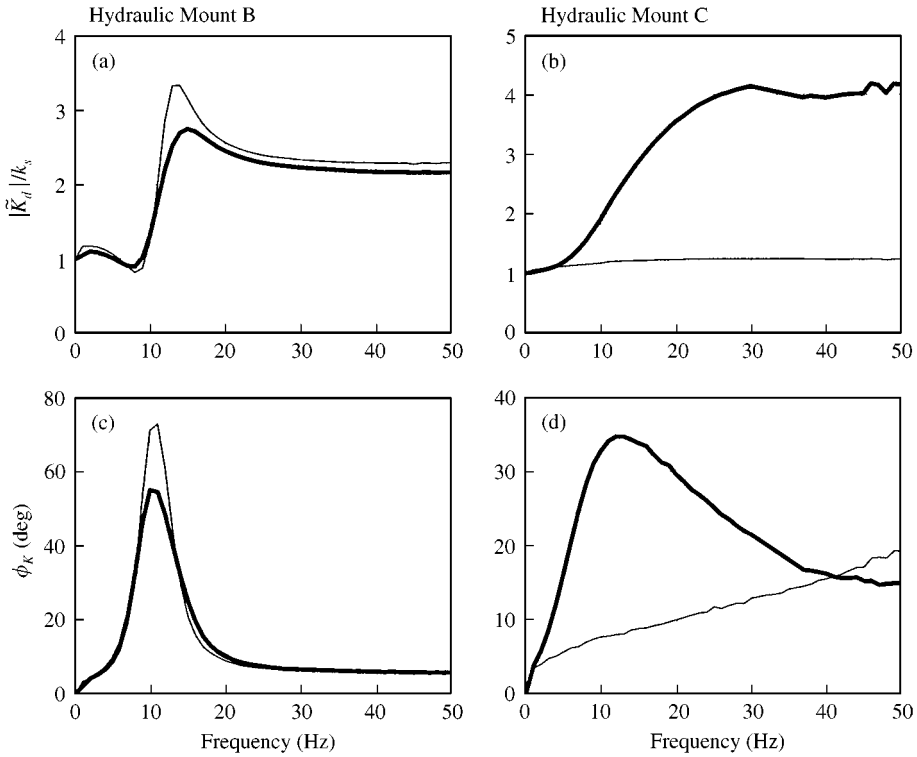


Figure 15. Measured dynamic stiffness of typical hydraulic mounts: —, $X = 0.125$ mm; - - -, $X = 0.5$ mm.

TABLE 6

Natural frequencies of the 1/2 car model of Figure 4 with hydraulic mount (B) data of Figure 19

Mode	Given static k_s	Natural frequencies (Hz)			
		Given dynamic \tilde{K}_d			
		$X = 0.125$ mm	$X = 0.25$ mm	$X = 0.375$ mm	$X = 0.50$ mm
1	1.1	$1.1 + 9.5e - 5i$	$1.2 + 8.5e - 5i$	$1.1 + 8.5e - 5i$	$1.1 + 7.3e - 3i$
2	8.4	$7.7 + 1.6i$	$7.8 + 1.7i$	$7.9 + 1.8i$	$8.0 + 2.0i$
3	8.8	$8.7 + 3.4e - 3i$	$8.7 + 3.8e - 3i$	$8.7 + 4.0e - 3i$	$8.7 + 4.2e - 3i$
4	11.2	$11.1 + 1.1e - 3i$	$11.1 + 1.2e - 3i$	$11.2 + 1.3e - 3i$	$11.1 + 1.4e - 3i$
5	15.4	$12.7 + 1.1i$	$12.6 + 1.4i$	$12.5 + 1.7i$	$12.3 + 2.0i$
6	24.1	$18.0 + 0.85i$	$18.0 + 0.93i$	$17.9 + 0.99i$	$17.8 + 1.0i$
7	—	$24.7 + 0.15i$	$24.7 + 0.16i$	$24.6 + 0.15i$	$24.6 + 0.15i$

multi-term harmonic balance technique depending on the non-linear characteristics or the accuracy needed.

A refined synthesis method, which incorporates local or sub-system non-linearities, is proposed here to fully understand the system behavior while providing an efficient calculation alternative especially for large structures. The generic non-linear system is defined exclusively in the frequency domain, as shown in Figure 17. Local non-linearities are introduced by N_M mounts that are located between two LTI sub-systems A and B of

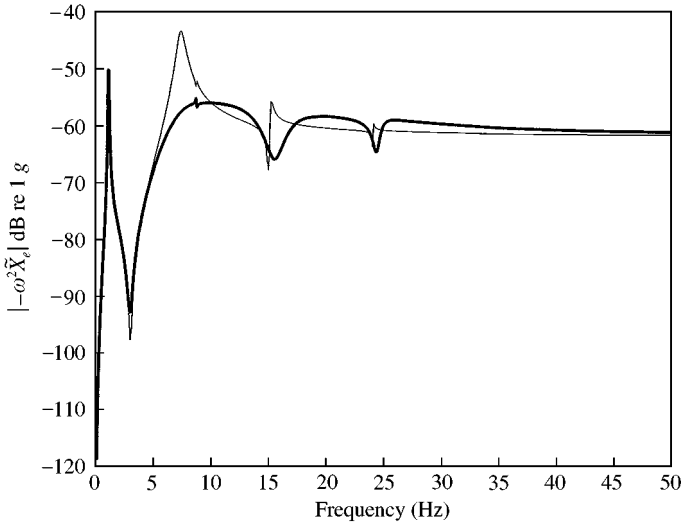


Figure 16. Effect of displacement amplitude (X) on engine acceleration for the 1/2 car model of Figure 4 with hydraulic mount (C) of Figure 15: —, $X = 0.125$ mm; - - -, $X = 0.5$ mm.

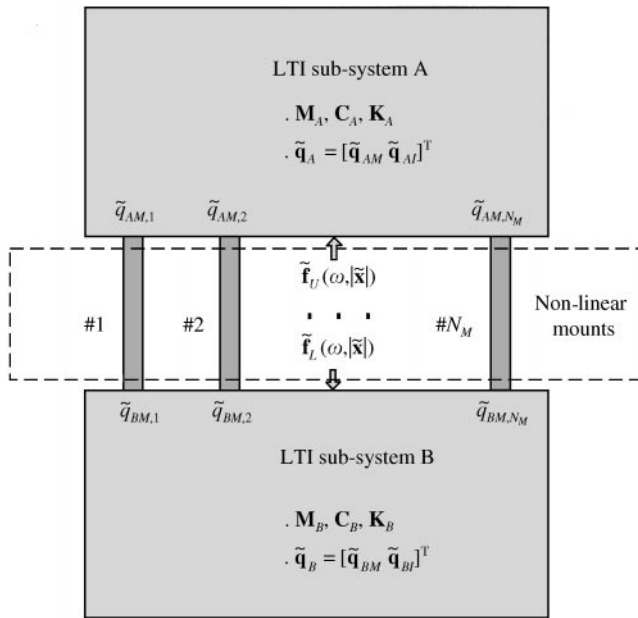


Figure 17. System synthesis concept that includes local non-linearities introduced by mounts.

dimensions N_A and N_B , respectively. For the given harmonic excitations $\tilde{\mathbf{f}}_A(\omega)e^{i\omega t}$ and $\tilde{\mathbf{f}}_B(\omega)e^{i\omega t}$, assume that only the harmonic responses are of interest: $\tilde{\mathbf{q}}_A(\omega)e^{i\omega t} = [\tilde{\mathbf{q}}_{AI}(\omega) \tilde{\mathbf{q}}_{AM}(\omega)]^T e^{i\omega t}$ and $\tilde{\mathbf{q}}_B(\omega)e^{i\omega t} = [\tilde{\mathbf{q}}_{BM}(\omega) \tilde{\mathbf{q}}_{BI}(\omega)]^T e^{i\omega t}$. Here the response $\tilde{\mathbf{q}}_A$ of sub-system A consists of $\tilde{\mathbf{q}}_{AM}$ that describes the interfacial regime with all mounts and $\tilde{\mathbf{q}}_{AI}$ for the remaining part. Similarly, $\tilde{\mathbf{q}}_B$ of sub-system B can be decomposed in terms of $\tilde{\mathbf{q}}_{BM}$ and $\tilde{\mathbf{q}}_{BI}$. The harmonic displacements across the mount are defined as $\tilde{\mathbf{X}}e^{i\omega t} = (\tilde{\mathbf{q}}_{AM} - \tilde{\mathbf{q}}_{BM})e^{i\omega t}$ and the non-linear interfacial forces are given by $\tilde{\mathbf{f}}_U(\omega, |\tilde{\mathbf{X}}|)e^{i\omega t} = -\tilde{\mathbf{K}}_M(\omega, |\tilde{\mathbf{X}}|)\tilde{\mathbf{X}}e^{i\omega t}$ and

$\tilde{\mathbf{f}}_L(\omega, |\tilde{\mathbf{X}}|)e^{j\omega t} = \tilde{\mathbf{K}}_M(\omega, |\tilde{\mathbf{X}}|)\tilde{\mathbf{X}}e^{j\omega t}$ that are exerted on A and B respectively. The governing equations of motion of the entire system are then assembled as follows:

$$[\mathbf{M}_A + i\omega\mathbf{C}_A + \mathbf{K}_A]\tilde{\mathbf{q}}_A(\omega, |\tilde{\mathbf{X}}|) = \tilde{\mathbf{f}}_A(\omega) + \mathbf{L}_{MA}^T\tilde{\mathbf{f}}_U(\omega, |\tilde{\mathbf{X}}|), \quad (30a)$$

$$[\mathbf{M}_B + i\omega\mathbf{C}_B + \mathbf{K}_B]\tilde{\mathbf{q}}_B(\omega, |\tilde{\mathbf{X}}|) = \tilde{\mathbf{f}}_B(\omega) + \mathbf{L}_{MB}^T\tilde{\mathbf{f}}_L(\omega, |\tilde{\mathbf{X}}|). \quad (30b)$$

Here, \mathbf{L}_{MA} is a Boolean selection matrix which extracts the interfacial d.o.f. from sub-system A (and likewise \mathbf{L}_{MB} is for B) and relates it to mounts. Now suppose that $\tilde{\mathbf{X}}$ is known (or assigned a specified value), then $\tilde{\mathbf{q}}_A$ and $\tilde{\mathbf{q}}_B$ can be expressed as $\mathbf{U}_A\tilde{\mathbf{p}}_A$ and $\mathbf{U}_B\tilde{\mathbf{p}}_B$ respectively, by using the modal expansion method since the left-hand sides of equations (30) possess only the LTI system property with proportionally damped \mathbf{C}_A and \mathbf{C}_B . Here, \mathbf{U}_A and \mathbf{U}_B represent the normal modal matrix for A and B while $\tilde{\mathbf{p}}_A$ and $\tilde{\mathbf{p}}_B$ represent the normal mode responses for A and B. Further define $\tilde{\mathbf{p}}_A$ and $\tilde{\mathbf{p}}_B$ as

$$\tilde{\mathbf{p}}_A(\omega, |\tilde{\mathbf{X}}|) = \text{diag}\left(\frac{1}{\omega_{A,k}^2 - \omega^2 + 2i\zeta_{A,k}\omega\omega_{A,k}}\right)\mathbf{U}_A^T(\tilde{\mathbf{f}}_A - \mathbf{L}_{MA}^T\tilde{\mathbf{K}}_M(\omega, |\tilde{\mathbf{X}}|)\tilde{\mathbf{X}}), \quad (31a)$$

$$\tilde{\mathbf{p}}_B(\omega, |\tilde{\mathbf{X}}|) = \text{diag}\left(\frac{1}{\omega_{B,k}^2 - \omega^2 + 2i\zeta_{B,k}\omega\omega_{B,k}}\right)\mathbf{U}_B^T(\tilde{\mathbf{f}}_B + \mathbf{L}_{MB}^T\tilde{\mathbf{K}}_M(\omega, |\tilde{\mathbf{X}}|)\tilde{\mathbf{X}}), \quad (31b)$$

where $\text{diag}(a_k)$ is a diagonal matrix with a_k as the k th element, $\omega_{A,k}$ is the k th natural frequency of sub-system A, $\zeta_{A,k}$ is the k th modal damping ratio of A; the same nomenclature is applied to sub-system B. If the assumed $\tilde{\mathbf{X}}$ is a valid solution, the responses $\tilde{\mathbf{q}}_{AM} = \mathbf{L}_{MA}\tilde{\mathbf{q}}_A$ and $\tilde{\mathbf{q}}_{BM} = \mathbf{L}_{MB}\tilde{\mathbf{q}}_B$ should be consistent with the values given by $\tilde{\mathbf{X}} = \tilde{\mathbf{q}}_{AM} - \tilde{\mathbf{q}}_{BM}$. Hence, the non-linear system problem can now be reformulated in terms of the following non-linear algebraic equation that must be iteratively solved for $\tilde{\mathbf{X}}$ at each ω :

$$\begin{aligned} &\tilde{\mathbf{X}}(\omega) - \mathbf{L}_{MA}\mathbf{U}_A \text{diag}\left(\frac{1}{\omega_{A,k}^2 - \omega^2 + 2i\zeta_{A,k}\omega\omega_{A,k}}\right)\mathbf{U}_A^T(\tilde{\mathbf{f}}_A(\omega) - \mathbf{L}_{MA}^T\tilde{\mathbf{K}}_M(\omega, |\tilde{\mathbf{X}}(\omega)|)\tilde{\mathbf{X}}(\omega)) \\ &+ \mathbf{L}_{MB}\mathbf{U}_B \text{diag}\left(\frac{1}{\omega_{B,k}^2 - \omega^2 + 2i\zeta_{B,k}\omega\omega_{B,k}}\right)\mathbf{U}_B^T(\tilde{\mathbf{f}}_B(\omega) + \mathbf{L}_{MB}^T\tilde{\mathbf{K}}_M(\omega, |\tilde{\mathbf{X}}(\omega)|)\tilde{\mathbf{X}}(\omega)) = 0. \end{aligned} \quad (32)$$

6.3. CONSTRUCTION OF A NON-LINEAR TIME DOMAIN MODEL

A time domain model for an amplitude- and frequency-dependent mount (say of Figure 1(b)) is first developed, based on a linear frequency-dependent model. For example, the model for Figure 2 with $X = 1.0$ mm was expressed by Singh *et al.* [10]

$$K_d(s) = \frac{f_M(s)}{x(s)} = k_r \left(\frac{s^2}{\omega_{n1}^2} + \frac{2\zeta_1 s}{\omega_{n1}} + 1 \right) \left/ \left(\frac{s^2}{\omega_{n2}^2} + \frac{2\zeta_2 s}{\omega_{n2}} + 1 \right) \right., \quad (33)$$

where s is the Laplace transformation variable. Equation (33) can be transformed to the corresponding time domain model as follows, where $f_T(t)$ is the transmitted force and $x(t)$ is the excitation, as shown in Figure 1(b):

$$\frac{1}{\omega_{n2}^2}\ddot{f}_T(t) + \frac{2\zeta_2}{\omega_{n2}}\dot{f}_T(t) + f_T(t) = k_r \left[\frac{1}{\omega_{n1}^2}\ddot{x}(t) + \frac{2\zeta_1}{\omega_{n1}}\dot{x}(t) + x(t) \right]. \quad (34)$$

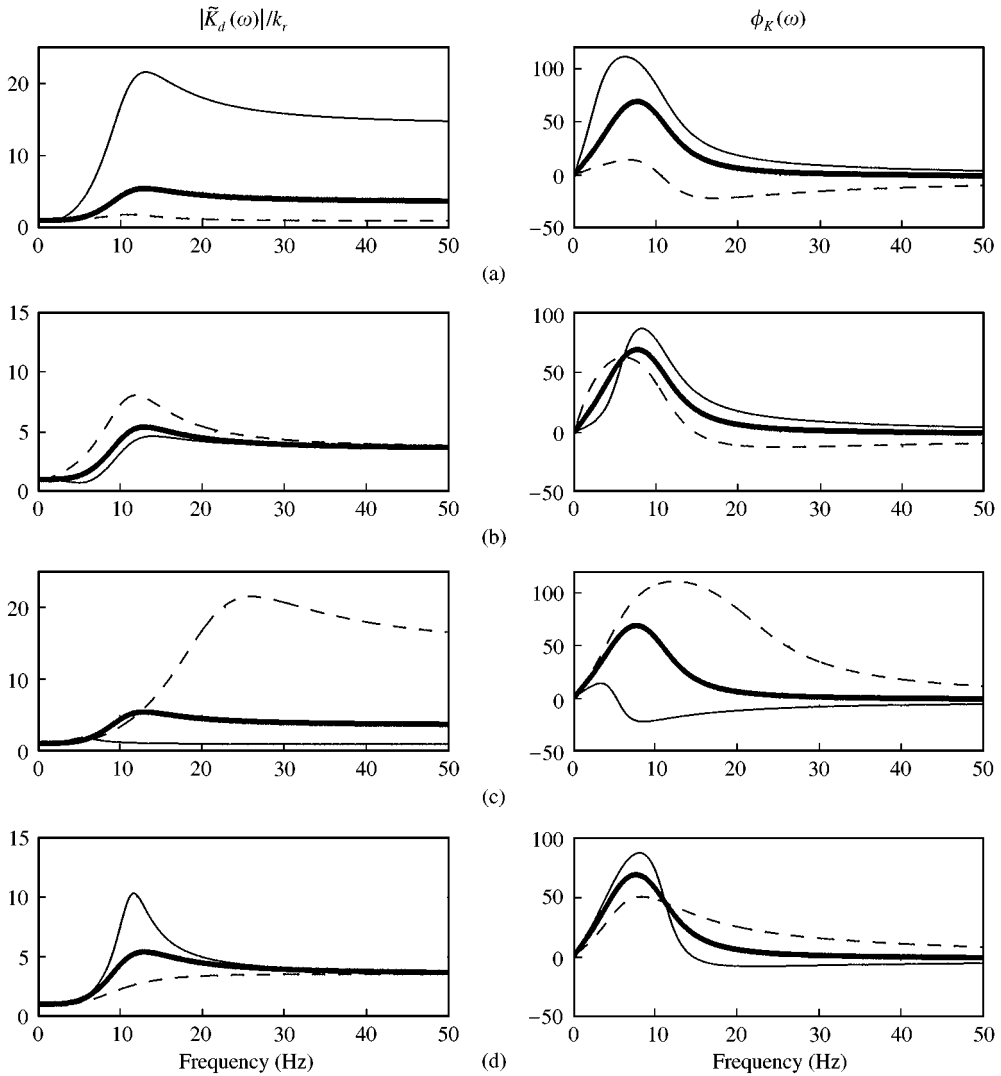


Figure 18. Effect of parameters on $\tilde{K}_d(\omega)$ as given by equation (34). (a) ω_{n1} , (b) ζ_1 , (c) ω_{n2} , and (d) ζ_2 : —, 50% of baseline value; —, baseline; ---, 200% of baseline value.

The amplitude-dependent model may now be empirically developed by observing the effects of ω_{n1} , ω_{n2} , ζ_1 , and ζ_2 on $K_d(s)$, given simulation or measured data, as shown in Figure 18. For example, the $\tilde{K}_d(\omega, X)$ at $X = 0.1$ mm of Figure 1(b) may be obtained by either increasing ω_{n1} or decreasing ω_{n2} . Hence, the non-linear equation for this mount is reformulated as follows where A_1 , A_2 , A_3 , and A_4 are empirical functions that assign amplitude-dependent properties:

$$\frac{1}{(A_3\omega_{n2})^2}\ddot{f}_T(t) + \frac{2(A_4\zeta_2)}{A_3\omega_{n2}}\dot{f}_T(t) + f_T(t) = k_r \left[\frac{1}{(A_1\omega_{n1})^2}\ddot{x}(t) + \frac{2(A_2\zeta_1)}{A_1\omega_{n1}}\dot{x}(t) + x(t) \right]. \quad (35)$$

In the time domain model, it is rather difficult to incorporate X as a variable. Therefore, the time history of $x(t) = X \sin(\omega t)$ is used as a criterion for selecting proper values of A_1 , A_2 ,

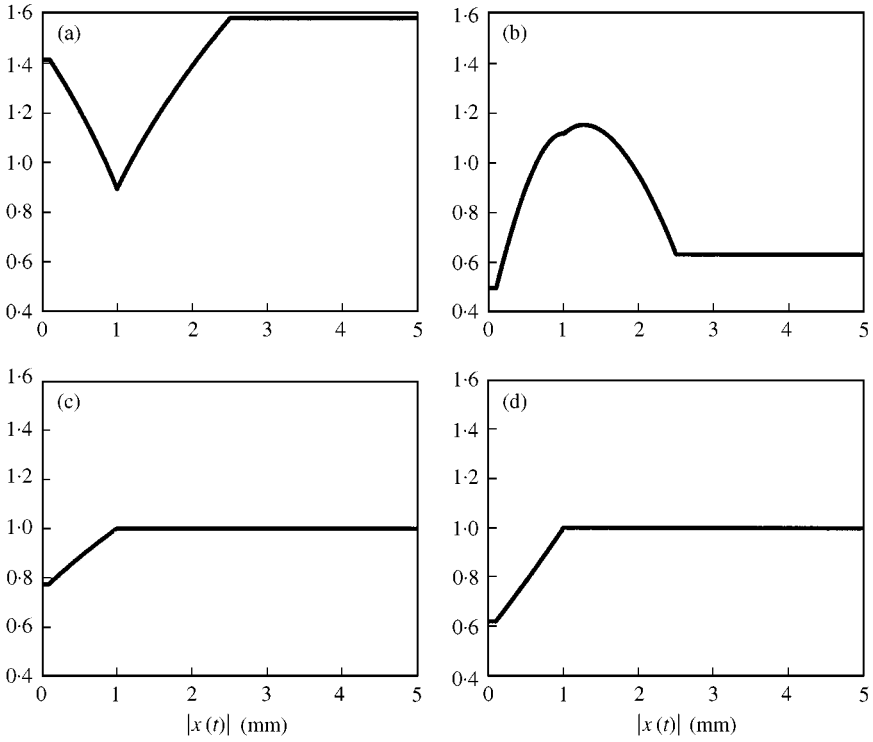


Figure 19. Empirical parameters of equation (35): (a) A_1 , (b) A_2 , (c) A_3 , (d) A_4 .

A_3 , and A_4 . Measured dynamic stiffness data of Figure 2 have the following amplitude-dependent characteristics. (a) From $X = 0.1$ to 1 mm, $|\tilde{K}_d(\omega)|$ and $\phi_K(\omega)$ increase until the maximum at $X = 1$ mm, and (b) when X exceeds 1 mm, $|\tilde{K}_d(\omega)|$ and $\phi_K(\omega)$ start decreasing. Four amplitude regimes are selected: $|x(t)| < 0.1$ mm, $0.1 \leq |x(t)| < 1$ mm, $1 \leq |x(t)| < 2.5$ mm, and $|x(t)| \geq 2.5$ mm. At each ω and X of $x(t) = X \sin(\omega t)$, $f_T(t) = f_{Ta} \sin(\omega t + \phi_K)$ is obtained by numerically integrating equation (35) and neglecting sub- and super-harmonic terms of $f_T(t)$. The dynamics stiffness $\tilde{K}_d(\omega, X)$ is then given by \tilde{f}_{Ta}/X . Figure 19 shows the plots of four empirical parameters for mount A that correspond to $\tilde{K}_d(\omega, X)$ of Figure 20. Since equation (35) is constructed purely for the sake of validation, it does not necessarily reproduce the results of Figure 2. Nonetheless, this formulation could clearly show the effects of ω and X for any mount.

6.4. 1/4-CAR EXAMPLE

Consider the 1/4 car of Figure 1(a) with parameters: $m_e = 122.3$ kg, $m_c = 270$ kg, $k_c = 20$ N/mm, and $b_c = 1400$ N s/m. The calculated $\tilde{K}_d(\omega, X)$ of Figure 20 which resembles the measured dynamic stiffness of mount A of Figure 2 is used for solving equation (32). Since the interfacial dimension is one, equation (32) is reduced to the following non-linear algebraic equation:

$$\left(-m_e \omega^2 + \frac{-(m_e + m_c)\omega^2 + ib_c \omega + k_c}{-m_c \omega^2 + ib_c \omega + k_c} \tilde{K}_d(\omega, X) \right) \tilde{X}(\omega) = f_a(\omega). \tag{36}$$

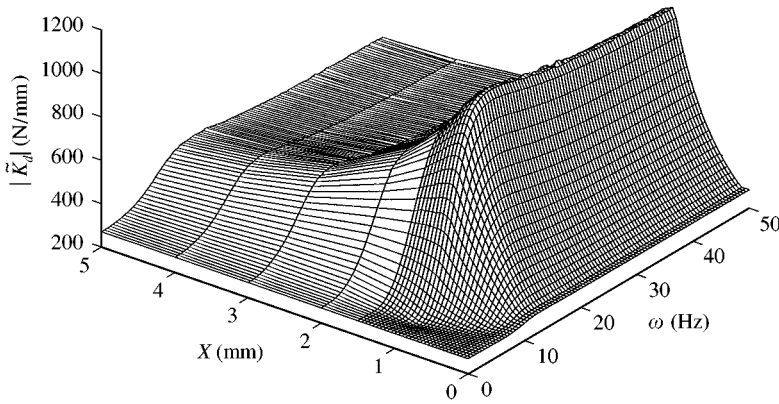


Figure 20. Dynamic stiffness calculated using equation (35).

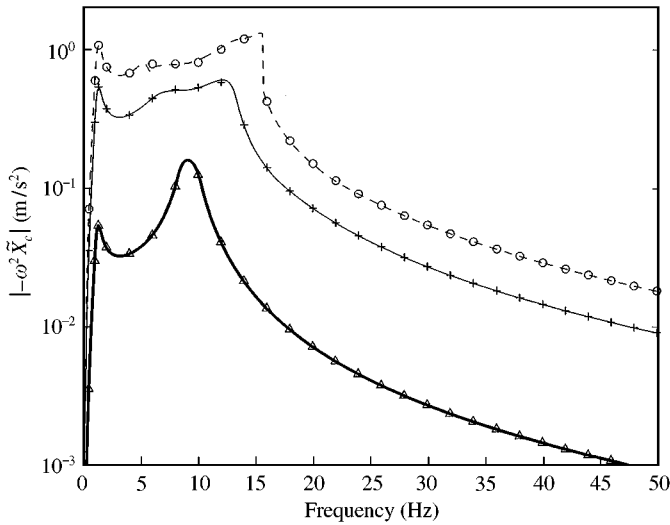


Figure 21. Comparison of chassis acceleration levels: time domain method (—, $|\tilde{f}_a| = 10$ N; —, $|\tilde{f}_a| = 100$ N; ---, $|\tilde{f}_a| = 200$ N) and frequency domain method (Δ , $|\tilde{f}_a| = 10$ N; +, $|\tilde{f}_a| = 100$ N; O, $|\tilde{f}_a| = 200$ N).

To provide $\tilde{K}_d(\omega, X)$ at any values of ω and X , one may resort to a surface fitting of Figure 20 by using bilinear, bicubic, or bispine interpolations. For the time domain analysis, the non-linear mount equation (35) is substituted into the 1/4 car system of Figure 1(a) and the resulting time domain model is as follows in terms of mount (or transmitted) $f_T(t)$ and excitation forces $f(t)$:

$$m_e \ddot{q}_e(t) + f_T(t) = f(t), \quad m_c \ddot{q}_c(t) + b_c \dot{q}_c(t) + k_c q_c(t) - f_T(t) = 0, \quad (37a,b)$$

$$\frac{k_r}{(A_1 \omega_{n1})^2} (\ddot{q}_e(t) - \ddot{q}_c(t)) - \frac{1}{(A_3 \omega_{n2})^2} \ddot{f}_T(t) + \frac{2k_r(A_2 \zeta_1)}{A_1 \omega_{n1}} (\dot{q}_e(t) - \dot{q}_c(t)) - \frac{2k_r(A_4 \zeta_2)}{A_3 \omega_{n2}} \dot{f}_T(t) + k_r (q_e(t) - q_c(t)) - f_T(t) = 0. \quad (37c)$$

For mount A of Figure 1, the relevant system parameters are $\omega_{n1}/(2\pi) = 6$ Hz, $\omega_{n2}/(2\pi) = 11.3$ Hz, $\zeta_1 = 0.66$, $\zeta_2 = 0.35$, and $k_r = 270$ N/mm. Predictions by equation (36) are compared with the results of equation (37) in Figure 21. To solve equation (36), the values of \tilde{K}_d at arbitrary points of ω and X are provided by using a bilinear interpolation. It is quite clear that the proposed frequency domain method matches extremely well with the time domain integration technique. Non-linear characteristics of the 1/4 car are clearly observed when the amplitude of excitation force $|\tilde{f}_a|$ is varied. The first resonance peaks in all cases appear around 1.2 Hz; it is associated with k_c and b_c which implies the vehicle suspension mode. But the second resonant peaks are observed around 9.5 Hz for $|\tilde{f}_a| = 10$ N, 13.4 Hz for 100 N, and 15.1 Hz for 200 N; it is associated with the engine bounce mode. One may also observe a hardening spring behavior since the backbone curves bend to the right. This has also been observed by Royston and Singh [35], based on a semi-analytical calculation method.

7. CONCLUSION

Five fundamental problems of frequency- and amplitude-dependent isolators, as shown in Table 1, have been defined and examined. Both linear and non-linear eigenvalue problems, as listed in Table 4, have been formulated to handle the frequency dependency of elastic and dissipative parameters. Real or complex eigensolutions may be obtained depending on the numerical values of parameters. Further, it has been found that the Type III model is better suited as an approximation when the visco-elastic damping is more dominant than the viscous damping in a physical system. In addition, error analyses reveal that the validity of the modal expansion method could be judged by using the error criterion ε_2^2 . Nonetheless, a more fundamental study is needed to better understand the nature of the non-linear eigenvalue problems. This work is left for a future project.

The application of the quasi-linear method to a 1/2 car model has revealed that frequency dependency may cause the frequency response functions to exhibit more peaks than system dimension would normally allow for an LTI system. This method is suitable to examine the global effects of the displacement excitation amplitude in a vehicle model, as shown in Figure 20. A refined non-linear synthesis method has been developed in the frequency domain, and has been validated by comparing to the corresponding time domain model. The proposed frequency domain formulation has distinct and pragmatic advantages over the true time domain models that are often not available for practical devices. Future studies may consider extending the synthesis method from a single-term to a multi-term harmonic balance technique. Numerical issues associated with the surface fitting of measured $\tilde{K}_d(\omega, X)$ need to be examined in detail. The use of the continuation method [47] could be implemented to trace the non-linear response curves.

ACKNOWLEDGMENT

The Chrysler Challenge Fund and the Goodyear Tire and Rubber Company (St. Marys) are gratefully acknowledged for supporting this research.

REFERENCES

1. J. HARRIS and A. STEVENSON 1987 *International Journal of Vehicle Design* **8**, 553–577. On the role of non-linearity in the dynamic behaviour of rubber components.
2. P. W. ALLEN, P. B. LINDELY and A. R. PAYNE 1966 *Use of Rubber in Engineering*. London: MacLaren and Sons Ltd.
3. A. R. PAYNE and J. R. SCOTT 1960 *Engineering Design with Rubber*. New York: Interscience Publishers Inc.

4. S. GADE, K. ZAVERI, H. KONSTANTIN-HANSEN and H. HERLUFSEN 1995 *Sound and Vibration* 16–19. Stress/strain measurements of viscoelastic materials.
5. E. F. GOBEL 1974 *Rubber Springs Design*. New York: Halsted Press.
6. A. N. GENT 1992 *Engineering with Rubber: How to Design Rubber Components*. New York: Hanser Publishers.
7. R. ORANGE 1999 *Experimental Characterization of Elastomers*. “Rubber & Hydraulic Mounts” short course at General Motors.
8. G. KIM and R. SINGH 1995 *Journal of Sound and Vibration* **179**, 427–453. A study of passive and adaptive hydraulic engine mount systems with emphasis on non-linear characteristics.
9. J. B. LAZAN 1968 *Damping of Materials and Members in Structural Mechanics*. New York: Pergamon Press.
10. R. SINGH, G. KIM and P. V. RAVINDRA 1992 *Journal of Sound and Vibration* **158**, 219–243. Linear analysis of an automotive hydro-mechanical mount with emphasis on decoupler characteristics.
11. N. O. MYKLESTAD 1952 *Transactions of the ASME, Journal of Applied Mechanics* **19**, 284–286. The concept of complex damping.
12. W. N. FINDLEY, J. S. LAI and K. ONARAN 1976 *Creep and Relaxation of Nonlinear Viscoelastic Materials*. New York: Dover Publications Inc.
13. A. L. KIMBALL and N. Y. SCHENECTADY 1929 *Transaction of ASME, Journal of Applied Mechanics* **51**, 227–236. Vibration damping, including the case of solid friction.
14. J. C. SNOWDON 1968 *Vibration and Shock in Damped Mechanical Systems*. New York: John Wiley & Sons, Inc.
15. A. D. NASHIF, D. I. G. JONES and J. P. HENDERSON 1986 *Vibration Damping*. New York: John Wiley & Sons, Inc.
16. C. T. SUN and Y. P. LU 1995 *Vibration Damping of Structural Elements*. Englewood Cliffs, NJ: Prentice-Hall PTR.
17. N. J. FERGUSSON and W. D. PILKEY 1992 *Transaction of ASME, Journal of Applied Mechanics* **59**, 136–139. Frequency-dependent element mass matrices.
18. T. E. ROOK and R. SINGH 1995 *Journal of Sound and Vibration* **182**, 303–322. Dynamic analysis of a reverse-idler gear pair with concurrent clearances.
19. A. H. NAYFEH and D. T. MOOK 1979 *Nonlinear Oscillation*. New York: John Wiley and Sons.
20. C. L. GAILLARD and R. SINGH 2000 *Applied Acoustics*. Dynamic analysis of automotive clutch dampers (in press).
21. S. NEUMARK 1957 *Reports and Memoranda-Aeronautical Research Council (Great Britain) No. 3269*. Concept of complex stiffness applied to problems of oscillations with viscous and hysteretic damping.
22. S. H. CRANDALL 1970 *Journal of Sound and Vibration* **11**, 3–18. The role of damping in vibration theory.
23. F. S. TSE, I. E. MORSE and R. T. HINKLE 1978 *Mechanical Vibrations: Theory and Applications*. Boston: Allyn and Bacon, Inc.
24. L. RAYLEIGH 1945 *Theory of Sound*, vol. 1. New York: Dover Publications, Inc.
25. T. K. CAUGHEY 1960 *Transaction of ASME, Journal of Applied Mechanics* **27**, 269–271. Classical normal modes in damped linear systems.
26. K. A. FOSS 1958 *Transaction of ASME, Journal of Applied Mechanics* **25**, 361–364. Coordinates which uncouple the equations of motion of damped linear dynamic systems.
27. G. PRATER, JR. and R. SINGH 1986 *Journal of Sound and Vibration* **104**, 109–125. Quantification of the extent of non-proportional viscous damping in discrete vibratory systems.
28. L. MEIROVITCH 1980 *Computational Methods in Structural Dynamics*. Maryland: Sijthoff & Noordhoff.
29. S. W. KUNG and R. SINGH 1998 *Journal of Sound and Vibration* **212**, 781–805. Vibration analysis of beams with multiple constrained layer damping patches.
30. R. M. LIN and M. K. LIM 1996 *Journal of Acoustical Society of America* **100**, 3182–3191. Complex eigensensitivity-based characterization of structures with viscoelastic damping.
31. J. S. PRZEMIENIECKI 1965 *Theory of Matrix Structural Analysis*. New York: Dover Publication Inc.
32. J. BRILLA 1997 *Meccanica* **32**, 187–195. Laplace transform and new mathematical theory of viscoelasticity.
33. J. S. BENDAT and A. G. PIERSOL 1986 *Random data Analysis and Measurement Procedures*. New York: John Wiley & Sons, Inc.
34. T. ROYSTON and R. SINGH 1996 *Journal of Sound and Vibration* **194**, 243–263. Periodic response of mechanical systems with local non-linearities using an enhanced Galerkin technique.

35. T. ROYSTON and R. SINGH 1997 *Journal of Acoustical Society of America* **101**, 2059–2069. Vibratory power flow through a nonlinear path into a resonant receiver.
36. J. M. CUSCHIERI 1992 *Journal of Acoustical Society of America* **91**, 2686–2695. Parametric analysis of the power flow on an L-shaped plate using a mobility power flow approach.
37. W. C. HURTY 1965 *AIAA Journal* **3**, 678–685. Dynamic analysis of structural systems using component modes.
38. A. L. HALE and L. MEIROVITCH 1980 *Journal of Sound and Vibration* **69**, 309–326. A general substructure synthesis method for the dynamic simulation of complex structure.
39. J. FARSTAD and R. SINGH 1995 *Journal of Acoustical Society of America* **97**, 2855–2865. Structurally transmitted dynamic power in discretely joined damped component assemblies.
40. J. FARSTAD and R. SINGH 1996 *Journal of Acoustical Society of America* **100**, 3144–3158. Effects of modal truncation errors on transmitted dynamic power estimates in discretely joined component assemblies.
41. T. E. ROOK and R. SINGH 1996 *Journal of Acoustical Society of America* **99**, 2158–2166. Modal truncation issues in synthesis procedures for vibratory power flow and dissipation.
42. J. W. DAVID and L. D. MITCHELL 1984 *Proceedings of the 2nd International Conference on Recent Advances in Structural Dynamics*, Vol. II, 271–280, *Institute of Sound and Vibration, Southampton, England*, 9–13 April. Extension of transfer–matrix methodology to nonlinear problems.
43. Y. REN and C. F. BEARDS 1994 *Journal of Sound and Vibration* **172**, 593–604. A new receptance-based perturbative multi-harmonic balance method for the calculation of the steady state response of non-linear systems.
44. A. N. JEAN and H. D. NELSON 1990 *Journal of Sound and Vibration* **143**, 389–473. Periodic response investigation of large order non-linear rotor dynamic system using collocation.
45. Y. K. CHEUNG, S. H. CHEN and S. L. LAU 1990 *Journal of Sound and Vibration* **140**, 273–286. Application of the incremental harmonic balance method to cubic non-linearity systems.
46. S. L. LAU and Y. K. CHEUNG 1981 *Transactions of the American Society of Mechanical Engineers, Journal of Applied Mechanics* **48**, 959–964. Amplitude incremental variational principle for nonlinear vibration of elastic systems.
47. C. PADMANABHAN and R. SINGH 1995 *Journal of Sound and Vibration* **184**, 35–38. Analysis of periodically excited non-linear systems by a parametric continuation technique.
48. R. J. COMPARIN and R. SINGH 1990 *Transactions of the ASME, Journal of Applied Mechanics* **112**, 237–245. An analytical study of automotive neutral gear rattle.
49. A. GELB and W. E. V. D. VELDE, 1968, *Multiple Input Describing Functions and Nonlinear System Design*. New York: McGraw-Hill.
50. M. URABE 1966 *Archives of Rational Mechanical Analysis*, 120–152. Galerkin's procedure for nonlinear periodic systems.
51. C. A. J. FLETCHER 1984 *Computational Galerkin Methods*. New York: Springer-Verlag.

APPENDIX A: NOMENCLATURE

a_1, a_2, a_3	coefficients of polynomial orders in $K'_d(\omega)$
b_1, b_2, b_3	coefficients of polynomial orders in $K''_d(\omega)$
$a(\omega)$	spectral function
A_1, A_2, A_3, A_4	amplitude-dependent non-linear parameters
A, B	system matrices in $2N$ space
b_c	viscous damping coefficient of chassis
c	viscous damping coefficient
C	viscous damping matrix
D	dynamic system (stiffness) matrix
f, g	force
F	external force amplitude
f, g	external force vector
i	$\sqrt{-1}$
k	stiffness
K_d	dynamics stiffness
K'_d	storage stiffness
K''_d	loss stiffness
K	stiffness matrix
L	Boolean selection matrix
m	mass

M	inertia matrix
N	dimension of a dynamic system
N', N''	number of polynomial orders in frequency-dependent mount
N_ω	number of frequency points in ε
p	modal displacement
p	modal displacement vector
q	generalized displacement
q	generalized displacement vector
R	random function
s	Laplace transformation variable
t	time
u, w	eigenvectors
U, W	modal matrices
x	displacement
x, y	displacement vector
X	displacement amplitude
α, β	Rayleigh's coefficients
δ_{ij}	Kroneker delta function
$\varepsilon_1, \varepsilon_2, \varepsilon_3, \varepsilon_4$	error criteria
Δ_d	decoupler gap
$\Gamma_{sd}, \Gamma_{sd2}$	scaling factor between static and storage stiffnesses
ϕ	phase angle
ϕ_K	loss angle or phase of dynamic stiffness
λ	eigenvalue
ω	frequency, rad/s
ϖ	non-dimensional frequency
ζ	viscous damping ratio
η	loss factor

Subscripts

a	amplitude
A	sub-system A
B	sub-system B
d	dynamic stiffness
e	engine or equivalent quantity
c	chassis
I	imaginary part or a sub-system component
k	index
$r, j = 1, 2, \dots, N$	modal indices
M	mount or modal domain
L	lower limit or lower interface of non-linear mount
H	upper limit
o	reference value
R	real part
s	static stiffness
T	transmitted quantity
U	upper interface of non-linear mount

Superscripts

T	transpose
\sim	complex valued
$-$	static load
$\hat{}$	approximate value

Operators

<i>diag</i>	diagonal matrix
Re	real part of complex variable
Im	imaginary part of complex variable
det	determinant of matrix
$\langle \rangle_\omega$	spectral average